SUPPLEMENTARY INFORMATION

Acetyl-CoA carboxylase 1 knockdown promotes esophageal squamous cell carcinoma metastasis via the CXCL8–NET axis

This file includes:

Materials and Methods

Supplementary Figure 1 to 9

Supplementary Table 1 to 6

Uncropped blot images

SUPPLEMENTARY METHODS

Cell culture

Human esophageal squamous cell carcinoma (ESCC) cell line KYSE-450 and KYSE-140 were obtained from Cobioer Bioscience (Nanjing, China), while ESCC cell line KYSE-150 and human embryonic renal cell line 293T were obtained from Cell Bank of the Typical Culture Preservation Committee of the Chinese Academy of Sciences (Shanghai, China). KYSE-450, KYSE-150, KYSE-140 were grown in RPMI 1640 (R10-040-cv-1803, Corning, Beijing, China), supplemented with 10% fetal bovine serum (FBS) (04-001-1A, VivaCell, Shanghai, China) and 1% penicillin-streptomycin solution (P/S) (P1400, Solarbio, Beijing, China). 293T cells were cultured in DMEM (10-013-CV, Corning, Beijing, China), also supplemented with 10% FBS and 1% P/S. The mycoplasma testing demonstrated no mycoplasma contamination using a mycoplasma detection kit (C0301S, Beyotime, Shanghai, China) (Supplementary Figure 9), and the STR sequencing (Personalbio, Shanghai, China) analysis confirmed the authenticity of the cell lines used in this study (Supplementary table. 5). To assess the impact of reparixin (S8640, Selleck, Houston, USA), LY294002 (S1737, Selleck, Houston, USA), U0126 (A1337, APExBIO, Houston, USA), and C646 (S7152, Selleck, Houston, USA) on the expression of EMT markers, ESCC cell lines were treated with 400 nM reparixin, 5 μM LY294002, 10 μM U0126, or 20 μM C646, along with the respective solvent controls for 24 h.

ACC1 knockdown cell line construction

shRNA sequences used were as follows: shNC: 5'-TTCTCCGAACGTGTCACGT-3'; shACC1: 5'-TACAAGGGATACAGGTATTTA-3'. KYSE-150 and KYSE-450 cells were seeded in 35-mm diameter cell culture dishes at a density of 3×10^5 cells per dish and cultured overnight. The next day, the medium was replaced with 1 ml of basic medium containing 5 μg/ml polybrene and 20 μl either shNC or shACC1 virus. After 24 h, the virus-containing medium was replaced with fresh complete medium, and cells were cultured for an additional 24 h. Subsequently, cells, including original KYSE-150 and KYSE-450 cells without virus infection, were cultured and screened with complete media containing 4 μg/ml puromycin. Once uninfected original cells were eliminated by puromycin, puromycin-resistant negative control cells (shNC) and ACC1 knockdown cells (shACC1) were cultured with 1 μg/ml puromycin continually for 2 weeks. KYSE-150 shNC/shACC1 and KYSE-450 shNC/shACC1 cells were obtained and the knockdown efficiency was confirmed by immunoblotting.

Luciferase cell line construction

Genechem (Shanghai, China) provided the lentiviral vector Ubi-MCS-firefly-luciferase-SV40-neomycin, which expresses the luciferase gene, as well as the virus packaging and preparation services. The viral titer was determined to be 1×10^8TU/ml. Cell inoculation and virus infection were performed following the same protocol as described for the construction of ACC1 knockdown cell line. Both treated cells and uninfected KYSE-150 cells were simultaneously cultured and subjected to selection with complete media containing 600 μg/ml of neomycin (S3028, Solarbio, Beijing, China). Upon complete elimination of uninfected KYSE-150 cells by

neomycin, neomycin-resistant cells expressing luciferase (luc) were cultured with 200 μg/ml neomycin continually for 2 weeks. KYSE-150-luc cells were obtained and confirmed using a Bioluminescence detector (Glomax Multi JR, Promega, Beijing, China).

ACC1 overexpression plasmid transfection

The plasmid pReceiver-M07 expressing a negative control (vector plasmid) or human full-length *ACC1* gene (ACC1 plasmid) was provided by Fulengene (Guangzhou, China). Vector and ACC1 plasmids were extracted using an endotoxin-free plasmid extraction kit (DP118, TIANGEN, Beijing, China), and their concentration and purity were measured using a microvolume spectrophotometer (NanoPhotometer® NP80, IMPLEN, München, Germany). For plasmid transfection and cell identification, KYSE-140 cells were seeded in a 35-mm diameter cell culture dish at a density of 4×10^5 cells and cultured overnight. The next day, cells were transfected with 2.5 μg vector plasmid or ACC1 plasmid using 5 μl of Lipo 2000 transfection reagent. After 24 h, KYSE-140-vector and KYSE-140-ACC1 cells were obtained and used for migration and invasion experiments, as well as western blot assay.

siRNA transfection

The following siRNA sequences were utilized:

siNC: 5'-UUCUCCGAACGUGUCACGUTT-3';

siCXCL8: 5'-CTTAGATGTCAGTGCATAA-3';

sic-Fos: 5'-ACUAGAAGAUGAGAAGUCCTT-3';

siP300: 5'-AGGAGGAAGAAGAGAGAAATT-3'.

KYSE-150 shNC/shACC1 and KYSE-450 shNC/shACC1 cells were seeded in a 35-mm diameter cell culture dish at a density of 3×10^5 cells and cultured overnight. Subsequently, cells were transfected with 5 μl of the respective siRNA using 5 μl of Lipo 2000 in 100 μl of Opti-MEM (31985070, Thermo Fisher, Massachusetts, USA). After 24 h, the siRNA-containing media were removed and cells were cultured in fresh complete medium for another 24 h. KYSE-150 shNC/shACC1 siNC/siCXCL8/ sic-Fos/siP300 or KYSE-450 shNC/shACC1 siNC/siCXCL8/sic-Fos/siP300 cells were obtained. The knockdown efficiency was confirmed by immunoblotting, and the transfected cells were subsequently used for migration and invasion experiments as well as for further western blot analysis.

Dual luciferase reporter assays

The plasmid used in this study included CMV enhancer-3flag-polyA-EF1A-zsGreen-sv40-puromycin, expressing either a negative control (c-Fos vector plasmid) or full-length c-Fos gene (c-Fos plasmid), and the MCS-firefly-Luciferase plasmid, expressing either a negative control (CXCL8 promoter vector plasmid) or CXCL8 promoter (CXCL8 promoter plasmid), as along with TK promoter-Renilla-luciferase, which expresses the Renilla gene (Renilla plasmid). These plasmids were provided by Genechem (Shanghai, China), and plasmid acquisition and concentration measurement were conducted as described in the ACC1 overexpression plasmid method. For luciferase assay, 293T cells were seeded at a density of 1×10^5 cells/well in 12-well plates 24 h before transfection. Cells were co-transfected with 500 ng/well reporter gene plasmids (c-Fos vector plasmid or c-Fos plasmid or CXCL8 promoter

vector plasmid or CXCL8 promoter plasmid) and 50 ng/well Renilla plasmid as an internal control reporter. After 36 h, cells were collected, and the Luciferase reporter assays were performed using the Dual Luciferase Reporter Gene Assay Kit (RG027, Beyotime, Shanghai, China) using a Bioluminescence detector (Glomax Multi JR, Promega, Beijing, China).

Peripheral blood neutrophil isolation

Peripheral blood with EDAT anticoagulant from healthy human donors was carefully layered on an equal volume of PolymorphPrep^{TM} solution (AXS-1114683, Cosmo Bio, Tokyo, Japan). The samples were then centrifuged at 500 × g for 30 min at room temperature with the centrifuge brake turned off. After centrifugation, the stratification of neutrophils was clearly visible, and the neutrophil layer was carefully collected. The collected cells were washed once with 5 ml PBS (PM5090, Coolaber, Beijing, China) and centrifuged at 500 × g for 5 min at room temperature. The supernatant was discarded, and 5 ml ACK lysing buffer (SL1070, Beyotime, Shanghai, China) was added to lyse red cells. Following incubation at room temperature for 10 min, the mixture was centrifuged again, the supernatant was discarded. The isolated neutrophils were resuspended in 1 ml of 1640 medium containing 1% FBS. The purity of isolated neutrophils was assessed by flow cytometry (BDFACSCalibur, BD, New York, USA) using CD16 antibody (E-AB-F1236C, Elabscience, Wuhan, China) staining, consistently yielding a purity exceeding 95%.

Transwell assays

For the neutrophil Transwell assay, 1×10^5 neutrophils were seeded in the upper chamber with a pore size of 5 μm (3421, Corning, New York, USA) and incubated for 4 h. In the low chamber, 650 μl CM collected from different cells was added, along with either CXCL8 antibody (4 μg/ml, 94407, Cell Signaling Technology, Danvers, MA, USA) or IgG antibody (4 μg/ml, 2729, Cell Signaling Technology, Danvers, MA, USA). Various inhibitors, including reparixin, PAD4 inhibitor GSK484 (PAD4i) (10 μM, GC19184, GLPBIO, Shanghai, China), neutrophil elastase inhibitor (NEi) (5 μM, GC19523, GLPBIO, Shanghai, China) or Dnase I (0.25 mg/ml, 11284932001, Roche, Shanghai, China), were added based on the experimental purpose. For the NETs-ESCC clusters [1] transwell assay, 1×10^4 ESCC cells were plated in the upper wells with a pore 8 μm and incubated for 24 h. Subsequently, 5×10^5 neutrophils mixed with 650 μl of CM were seeded in the lower chamber, and different inhibitors, including reparixin, PAD4i, NEi or Dnase I, were added based on the experimental purpose. Following incubation, the penetrated cells from the upper surface of the membrane were wiped off, and the cells that crossed the membrane were fixed with 4% paraformaldehyde (BL539A, Biosharp, Beijing, China) and stained with crystal violet (G1062, Solarbio, Beijing, China). The number of penetrated cells was counted under a light microscope (ECLIPSE Ts2, Nikon, Tokyo, Japan) in five views of transwell (top, bottom, left, right, and center), and the average cell coverage was calculated. Quantitative analysis of the migration and invasion assays was performed using Image J software. Statistical significance was determined by comparing the means of the triplicate experiments.

Induction and identification of NETs in Vitro

Human neutrophils at 1×10^5 were plated on cell slides in 24-well plate and mixed with 500 μl CM collected from shNC/shACC1 cells. CXCL8 antibody (4 μg/ml) or IgG (4 μg/ml) antibody, as well as different inhibitors including PAD4i (10 μM), NEi (5 μM), and Dnase I (0.25 mg/ml), were added based on the experimental purpose. After co-culture for 4 h, the cell slides were collected and fixed in 4% paraformaldehyde for 15 min. Neutrophils treated with PMA (100 μg/ml, sc-3576A, Santa Cruz, California, USA) were used as a positive control for NETs formation. Subsequent fluorescent staining was performed.

Western blot

The antibody information is shown below: anti-ACC1 (1:1000, 4190, Cell Signaling Technology, Danvers, MA, USA), anti-H3K9ac (1:1000, 9649, Cell Signaling Technology, Danvers, MA, USA), anti-H3 (1:1000, 4499, Cell Signaling Technology, Danvers, MA, USA), anti-c-Fos (1:1000, 66590-1-Ig, Proteintech, Wuhan, China), anti-CXCL8 (1:1000, 94407, Cell Signaling Technology, Danvers, MA, USA), anti-p-AKT (1:1000, 4060, Cell Signaling Technology, Danvers, MA, USA), anti-AKT (1:1000, 4691, Cell Signaling Technology, Danvers, MA, USA), anti-p-ERK1/2 (1:2000, 4370, Cell Signaling Technology, Danvers, MA, USA), anti-ERK1/2 (1:2000, 4695, Cell Signaling Technology, Danvers, MA, USA), anti-PAI-1 (1:1000, WL01486, Wanlei, Shenyang, China), anti-Slug (1:2000, 9585, Cell Signaling Technology, Danvers, MA, USA), anti-Vimentin (1:1000, WL00742,

Wanlei), anti-E-cadherin (1:2000, 3195, Cell Signaling Technology, Danvers, MA, USA), anti-β-actin (1:2000, 4967, Cell Signaling Technology, Danvers, MA, USA).

cDNA preparation and quantitative real-time PCR

Paired primers for indicated genes in this study were described below.

CXCL8 forward primer: ACTGAGAGTGATTGAGAGTGGAC;

CXCL8 reverse primer: AACCCTCTGCACCCAGTTTTC.

ACC1 forward primer: ATCCCGTACCTTCTTCTACTG;

ACC1 reverse primer: CCCAAACATAAGCCTTCACTG.

c-Fos forward primer: CACTCCAAGCGGAGACAGAC;

c-Fos reverse primer: AGGTCATCAGGGATCTTGCA

GAPDH forward primer: GGAGCGAGATCCCTCCAAAAT;

GAPDH reverse primer: GGCTGTTGTCAT ACTTCTCATGG.

CXCL8 Site1 ChIP forward primer: CCTACAATAAGGGACAT;

CXCL8 Site1 ChIP reverse primer: TACACTGAATTCTATAGC.

CXCL8 Site2 ChIP forward primer: GTCCTTACATTGCTTT;

CXCL8 Site2 ChIP reverse primer: AGAGTGAAGGGGCACA.

CXCL8 Site3 ChIP forward primer: TGTGGAGCTTCAGTATTT;

CXCL8 Site3 ChIP reverse primer: AGGGCAAACCTGAGTCATC.

In our qPCR analysis of clinical samples, patients with overall survival (OS) ≥ 60 months (5 years) were classified as the favorable prognosis group, while those with OS ≤14 months (1.16 years) were categorized as the poor prognosis. The deviation of our poor prognosis definition (OS ≤ 14 months) from the conventionally used

threshold (OS ≤ 12 months) was deliberate and driven by considerations of sample size balance and statistical power within our cohort. The rationale is detailed below: Initial stratification using strict criteria (Favorable: OS ≥ 60 months; Poor: OS ≤ 12 months) revealed a significant imbalance in group sizes: the poor prognosis group (OS ≤ 12 months) contained substantially fewer patients than the favorable prognosis group (OS ≥ 60 months). To enhance group comparability, improve statistical power, and increase the reliability of comparisons, we implemented a minimal, justified expansion of the poor prognosis group inclusion criteria. Specifically, the upper limit for poor prognosis was extended from OS = 12 months to OS = 14 months. This adjustment incorporated only 8 additional patients with survival times between >12 and ≤14 months (i.e., 12 < OS ≤ 14) into the poor prognosis group. We contend that the prognosis for patients surviving 12-14 months remains clinically unfavorable, justifying their classification within the "poor prognosis" category. This adjustment was deliberate and minimal (spanning only 2 months), implemented specifically to address the sample size imbalance while preserving the clinical relevance of the group definitions.

CXCL8 enzyme-linked immunosorbent assay (ELISA)

The levels of CXCL8 secreted into the CM were quantified using a Human CXCL8 PicoKine ELISA kit (EK0413, Boster, Wuhan, China) according to the manufacturer's protocol. The absorbance was measured at 450 nm using a microplate spectrophotometer (BioTek Epoch 2, Agilent Technologies, Santa Clara, CA, USA) to determine the optical density (OD). The OD values were then used to calculate the

concentration of CXCL8, based on a standard curve generated from known concentrations of recombinant CXCL8.

Measurement of cellular acetyl-CoA level

The Acetyl-CoA assay kit (MAK039, Sigma-Aldrich, St. Louis, MO, USA) was used to measure acetyl-CoA levels in cell culture medium following the manufacturer's instructions. Cells were cultured in 10-cm dishes until they reached approximately 80% confluence, at which point they were lysed using 500 µl of SDS-free lysate. After centrifugation, the supernatant was harvested, and 40 µl of 1.0 M perchloric acid (PCA) was added to remove proteins from the samples. Then, 3 M $KHCO_3$ was added to adjust the supernatant to a pH between 6-8. A standard curve was generated, and acetyl-CoA levels in the supernatant were determined using a fluorometric product ((λ excitation/emission = 535/587 nm) detected with a Gemini XPS Microplate Reader (Molecular Devices, San Jose, CA, USA). Acetyl-CoA was quantified based on the formula described in the manufacturer's instructions.

Immunohistochemistry

The tissue was initially fixed in 4% formaldehyde for 24 h at 4°C. The paraffin-embedded tissue was sliced to a thickness of 4 µm using a paraffin slicing machine (HistoCore BIOCUT, Leica, Wetzlar, Germany). Then the sections were deparaffinized and rehydrated before undergoing antigen retrieval in sodium citrate buffer at 100°C for 10 min. The sections were then permeabilized with 0.2% Triton X-100 for 10 min. After blocking with 10% bovine serum albumin (BSA) for 1 h at room temperature, the sections were incubated overnight at 4°C with primary

antibodies, including anti-Ly6G (1:500, 87048, Cell Signaling Technology, Danvers, MA, USA), anti-Cit-H3 (1:1000, ab5103, Abcam, Cambridge, UK), anti-MPO (1:1000, AF3667, R&D Systems, Minneapolis, MN, USA), anti-ACC1 (1:200, 4190S, Cell Signaling Technology, Danvers, MA, USA). This was followed by incubation with HRP-conjugated secondary antibody for 30 min at room temperature. The color reaction was performed with a DAB reagent from the Immunohistochemical staining kit (GK500705, Genetech, Shanghai, China). Images were acquired using a standing biological microscope (DM4B, LEICA, Wetzlar, Germany), and the number of positive cells was evaluated based on at least three representative images per sample.

Immunofluorescence staining

The lung tissue was initially fixed in 4% formaldehyde for 24 h at 4°C, followed by two washes with PBS., Then, the tissue was dehydrated in 15% and 30% sucrose solutions, and embedded in OCT (4583, Sakura Finetek USA, Inc., Torrance, CA, USA). Slices with a thickness of 10 μm were prepared using a freezing microtome (CM1950, Leica, Wetzlar, Germany). Sections of lung tissue were permeabilized with 0.2% Triton X-100 for 10 min at room temperature. Subsequently, they were blocked with 10% BSA for 1 h at 26°C and incubated at 4°C overnight with primary antibodies, including anti-Cit-H3 (1:1000, ab5103, Abcam, Cambridge, UK), anti-MPO (1:1000, AF3667, R&D Systems, Minneapolis, MN, USA). After washing with PBS, the sections were incubated with Alexa Fluor 594 (1:500, 150132, Abcam, Cambridge, UK) or Alexa Fluor 488 conjugated secondary antibodies (1:500, 150073, Abcam, Cambridge, UK) for 1 h at room temperature. Nuclei were stained with DAPI

(C0060, Beyotime, Shanghai, China) for 4 min at room temperature. Images were acquired using a confocal microscope (NikonAX, Nikon, Tokyo, Japan), and the number of positive cells was evaluated based on at least three representative images per sample.

Animal models

For the subcutaneously mouse model, 5×10^6 KYSE-150 shNC/shACC1 cells were suspended in 100 μl PBS and injected subcutaneously into the lateral thigh of the right in nude mouse. Tumor development was monitored every 3 days. Tumor volume was calculated using the formula Volume = 0.5 × Length (L) × Width^2 (W), where L represented the longest size and W represented the shortest size. After 21 days, the mouse were sacrificed, tumor tissues were harvested, photographed, weighed, and then divided into halves. One half was fixed with formaldehyde for subsequent staining, while the other half was frozen with liquid nitrogen for subsequent protein and RNA extraction.

For the tail vein mouse model, 1.75×10^6 KYSE-150-luciferase shNC/shACC1 cells were injected through tail vein of nude mouse. Ten days after injection, the mouse were intraperitoneally injected with GSK484 at 5 mg/kg in 200 μl or vehicle control every 3 days and weighed until the endpoint of the experiment. The metastasis progress was detected at 24 days after intraperitoneal injection of 150 mg D-luciferin (Beyotime, Shanghai, China) with a volume of 200 μl. After gaseous anesthesia with isoflurane, mouse were placed in AniView600 multi-mode animal imaging instrument (Biolight Biotechnology, Guangzhou, China) to detect the firefly bioluminescence

signals for monitoring metastasis progression. Following in vivo imaging, cardiac perfusion was performed, and lung tissue was obtained for immunofluorescence staining, and liver, kidney, and spleen tissue was obtained for HE staining.

In the subcutaneous mouse model experiment, 7 mouse were allocated to each group, totaling 14 mouse. For the tail vein mouse model experiment, 3 mouse were allocated to each of the four groups, totaling 12 mouse. Overall, a total of 26 mouse were used in all experiments. The individual mouse was considered the experimental unit within the studies.

Anesthesia method: All animals were anesthetized using inhaled isoflurane (R510-22-10, RWD, Shenzhen, China) through animal anesthetic system (R500, RWD, Shenzhen, China) at a concentration of 3%. The depth of anesthesia was continuously monitored during the experiment by observing respiratory rate and reflex responses, ensuring that the animals remained pain-free throughout the in vivo imaging. Euthanasia method: At the conclusion of the experiments, all animals were euthanized using cervical dislocation. This procedure was performed by experienced personnel following the loss of consciousness, ensuring that the animals were euthanized swiftly and humanely.

The animals were included in the subcutaneous mouse model if a palpable tumor formed within 7 days after injection of KYSE-150 shNC/shACC1 cells, and excluded if there were injection-site infections, no tumor growth over 14 days, or premature death before day 21. In the tail vein mouse model, the animals were included if there

were no immediate adverse reactions at the injection site, but excluded if the injection failed or the animal died within 7 days post-injection.

In the animal experiment of this study, the following two outcome indicators were defined: Metastasis area/lung area%: The lung tissue sections of mouse were observed and analyzed. The area of metastatic nodules formed by esophageal cancer cells in the lung tissue and the area of the entire lung tissue section were measured using image analysis software. The percentage of the metastatic nodule area to the lung tissue section area was calculated. This indicator directly reflects the extent of esophageal cancer cell metastasis in the lungs, with higher values indicating more severe metastasis. Metastatic nodules in lung tissue sections were examined under a microscope, and the number of nodules formed by esophageal cancer cells was counted by a pathologist. This metric directly reflects both the extent and severity of lung metastasis, with higher values corresponding to more pronounced metastasis.

The nude mouse model was selected for this study due to its immunodeficient nature, which prevents the rejection of human-derived KYSE-150 xenografts. This model directly addresses our scientific objectives by providing a robust in vivo system to quantitatively assess the specific role of ACC1 in primary tumor growth and distant metastasis. The relevance to human biology is underscored by the use of human cancer cells, and the processes of tumor proliferation and metastatic colonization observed recapitulate key aspects of human disease. However, certain limitations must be acknowledged. The immunocompromised state of the nude mouse precludes the investigation of critical interactions between the tumor and the adaptive immune

system, which is a central component of human cancer biology and therapy. Additionally, the subcutaneous tumor microenvironment differs from the esophageal site, potentially influencing tumor biology and drug responses. Despite these limitations, which are inherent to many xenograft models, our findings provide compelling preliminary evidence of ACC1's function in vivo and its potential as a therapeutic target for human cancers, justifying future studies in more complex, immunocompetent models.

In our study, the investigator was blinded to group allocations during treatment and outcome assessments to avoid bias and ensure objective data evaluation, six different investigators were involved in the animal experiments as follows: Investigator Jiaping Tang allocated treatments based on a randomization table and was the only one aware of the treatment group assignments. Investigator Qingya Zhuo performed the anesthesia. Investigators Shuhua Huo and Xinchen Dang were responsible for imaging and sample collection. Investigators Tianbao Pang and Kexin Cao, who were blinded to the treatment, assessed outcomes such as body weight, ESCC metastases in lung tissues, and tumor weight.

Patient inclusion and exclusion criteria

All patients included in this study underwent radical resection for ESCC without receiving preoperative radiotherapy or chemotherapy. Postoperative tissue samples were pathologically confirmed as ESCC. Patient selection was conducted in strict accordance with predefined inclusion and exclusion criteria. The inclusion criteria were: (1) patients with distinct prognoses who underwent surgery from January 1,

2014 to December 31, 2017; and (2) patients diagnosed with stage I–III ESCC. The exclusion criteria were: 1) incomplete clinical data, 2) postoperative complications, 3) missing tissue samples, and 4) deaths unrelated to tumor progression.

Determination of sample size

G*Power 3.1.9.7 software was utilized for sample size calculation, with a significance level (α) of 0.05 and statistical power (1-β) set at 0.8. The required sample size was determined based on data from previous studies, along with the standard deviation and effect size derived from long-term ESCC model preparation. Clinical samples, selected from patients with significant prognostic differences, were screened using specific inclusion and exclusion criteria between January 1, 2014, and December 31, 2017. The calculated sample size was sufficient to address the clinical questions and ensure statistical validity. To confirm reliability, we conducted interim and final power analyses, which indicated that the sample size and power level were appropriate for achieving statistically significant results.

REFERENCES

1. Xia X, Zhang Z, Zhu C, Ni B, Wang S, Yang S, et al. Neutrophil extracellular traps promote metastasis in gastric cancer patients with postoperative abdominal infectious complications. Nat Commun **13**, 1017 (2022)

Supplementary Figure 1

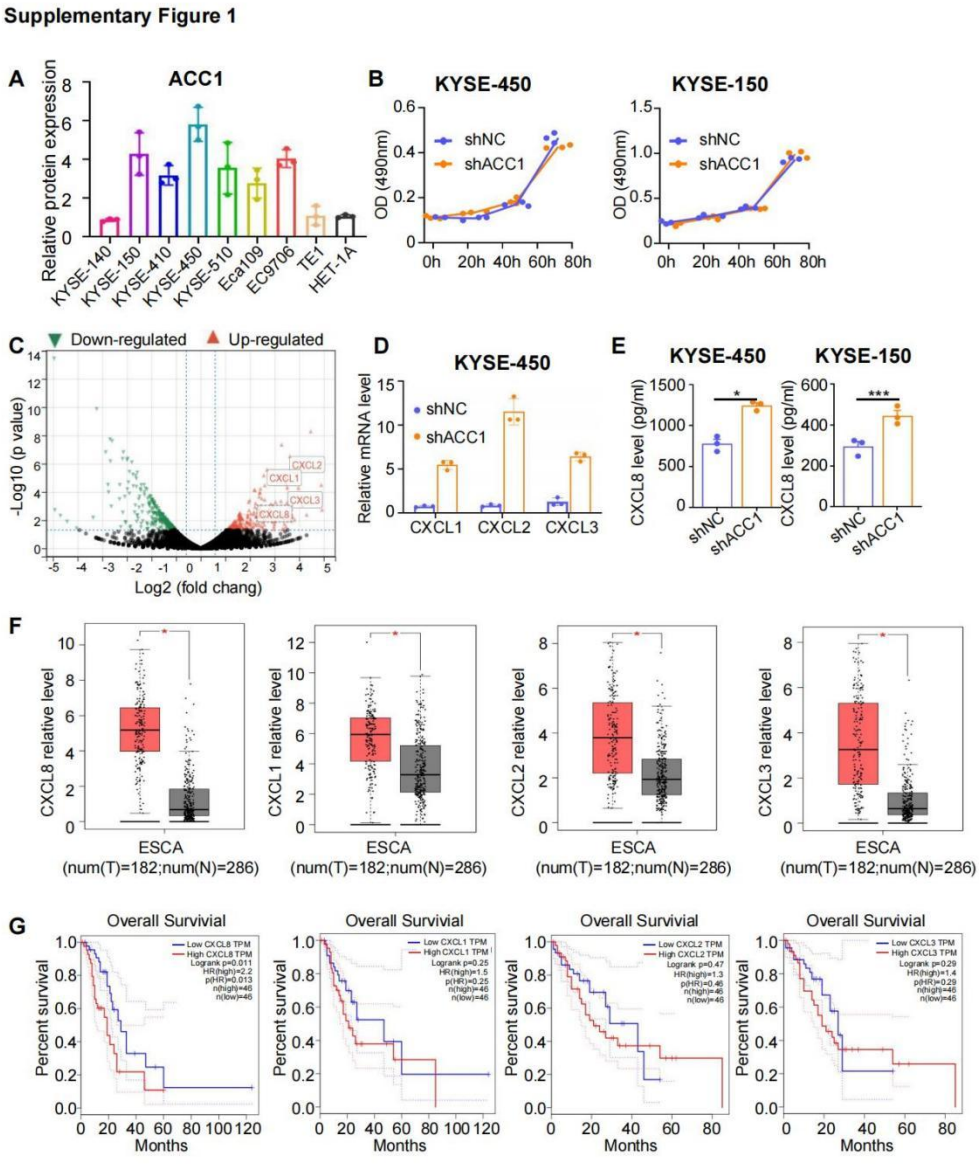

Supplementary Figure 1: ACC1 knockdown promotes ESCC cell migration and invasion by up-regulating CXCL8 expression. A ACC1 expression levels across various ESCC cell lines. **B** Cell viability of KYSE-450 shNC/shACC1 and KYSE-150 shNC/shACC1 cells determined using the MTT assay. **C** RNA-seq results indicating up-regulation of *CXCL1*, *CXCL2*, *CXCL3*, and *CXCL8* following ACC1 knockdown. **D** RT-qPCR analysis of *CXCL1*, *CXCL2*, and *CXCL3* expression levels

in KYSE-450 shNC/shACC1 cells. **E** ELISA assays measuring CXCL8 levels in CM from KYSE-450 shNC/shACC1 and KYSE-150 shNC/shACC1 cells. **F** CXCL8 expression levels in tumor tissues compared to adjacent tissues based on TCGA database data. **G** Kaplan-Meier survival analysis of esophageal cancer patients, comparing overall survival with high or low expression levels of CXCL8, CXCL1, CXCL2, and CXCL3 from the TCGA database. Each experiment was repeated thrice. Data are presented as mean ± SD. Significance levels are indicated as follows: $*P < 0.05$, $**P < 0.01$, $***P < 0.001$.

Supplementary Figure 2

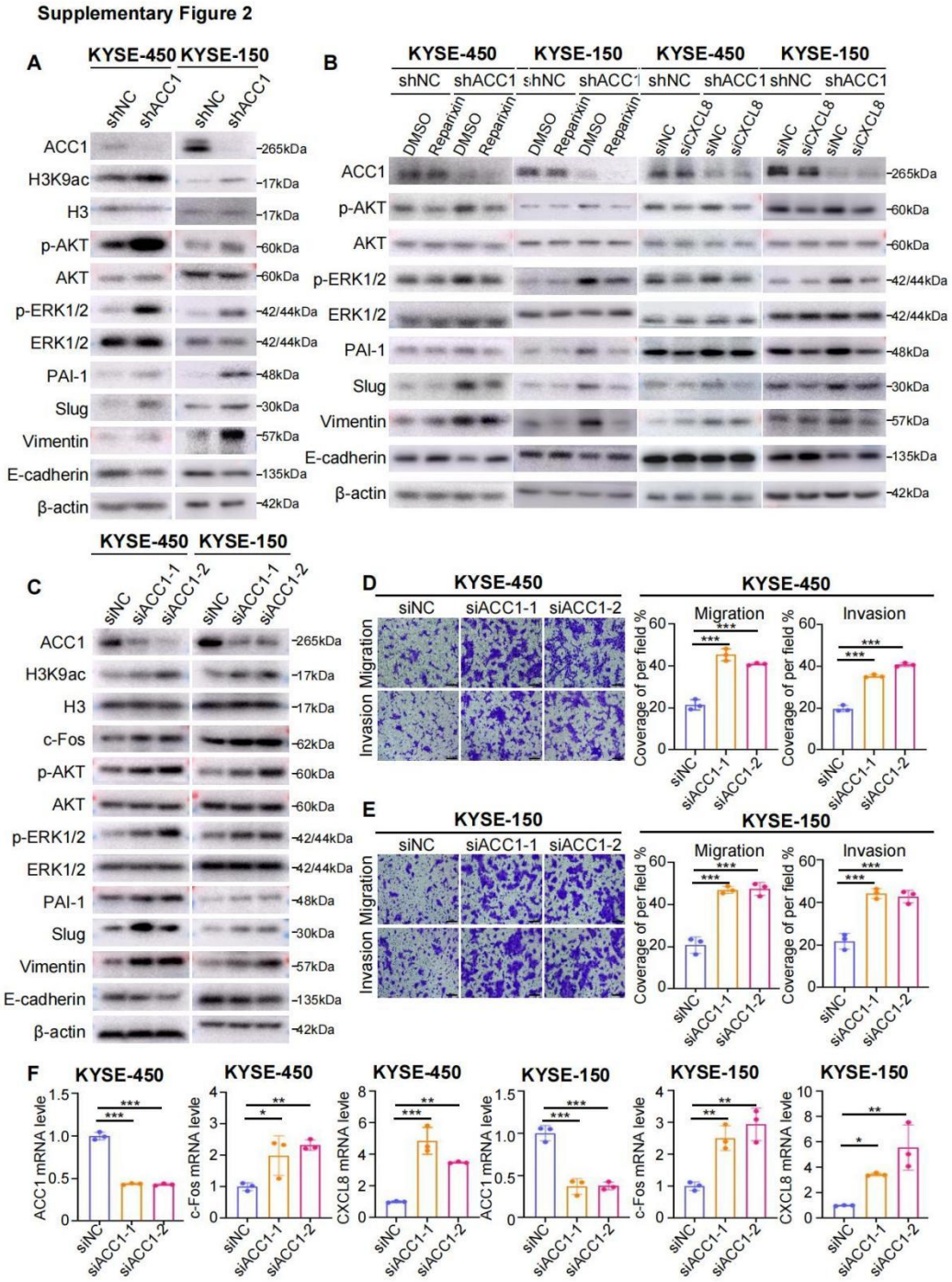

Supplementary Figure 2: ACC1 knockdown promotes migration and invasion by activating PI3K/AKT and MEK/ERK1/2 signaling pathways via CXCL8-CXCR1/2 signaling. A Immunoblot analysis demonstrating the impact of

ACC1 knockdown on the levels of p-ERK1/2, p-AKT, H3ac, and EMT marker proteins in KYSE-450 shNC/shACC1 and KYSE-150 shNC/shACC1 cells. **B** Immunoblot analysis illustrating the effects of reparixin and siCXCL8 on the levels of p-AKT, p-ERK1/2, and EMT marker proteins in KYSE-450 shNC/shACC1 and KYSE-150 shNC/shACC1 cells. **C** Immunoblot analysis demonstrating the impact of ACC1 knockdown on the levels of p-ERK1/2, p-AKT, H3ac, and EMT marker proteins in KYSE-450 siNC/siACC1 and KYSE-150 siNC/siACC1 cells. **D-E** Representative images and statistical analysis of migration and invasion in KYSE-450 siNC/siACC1 cells and KYSE-150 siNC/siACC1 cells. **F** RT-qPCR assays assessing the levels of *ACC1*, *c-Fos*, *CXCL8* in KYSE-450 siNC/siACC1 cells and KYSE-150 siNC/siACC1 cells.

Supplementary Figure 3

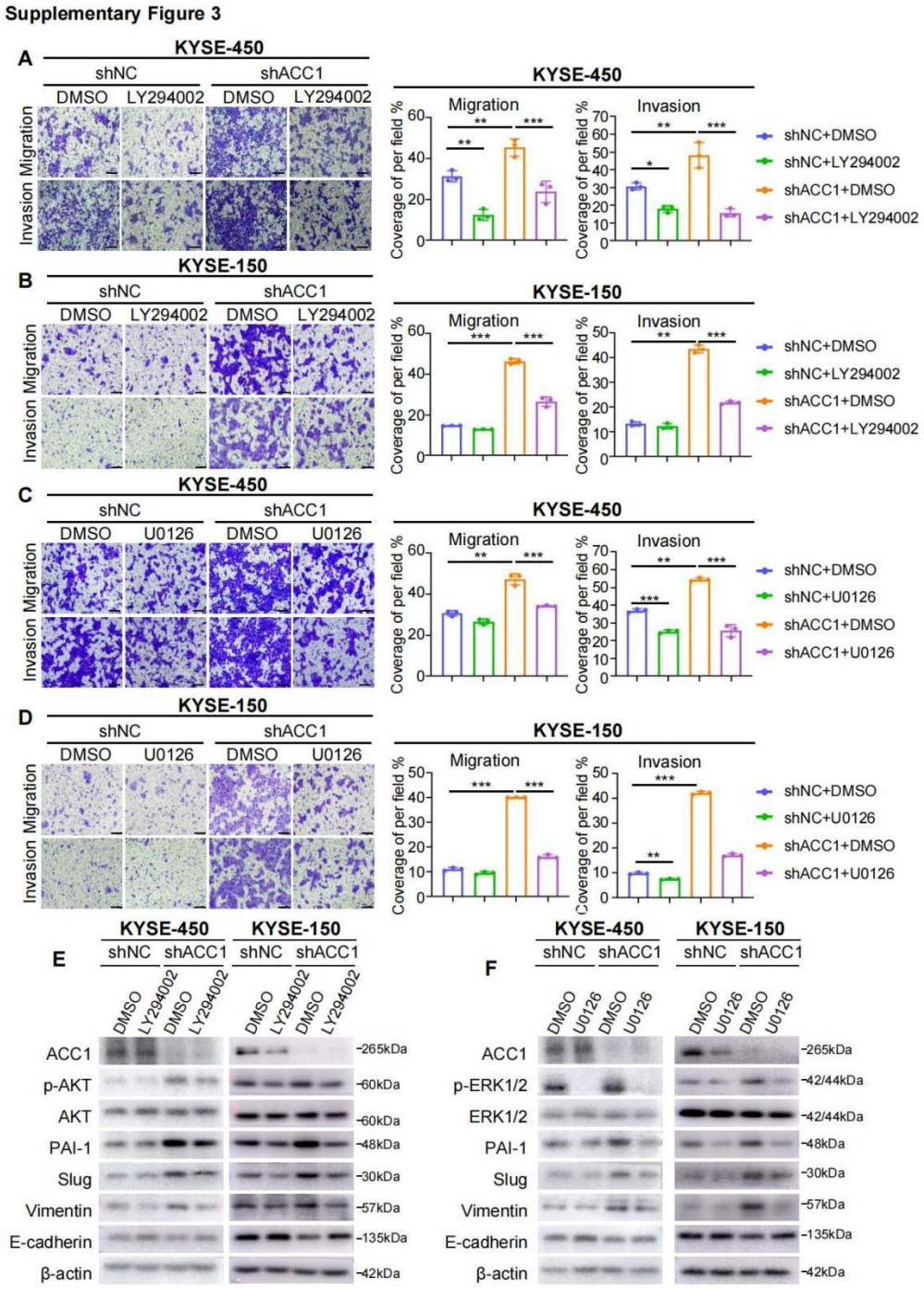

Supplementary Figure 3: ACC1 knockdown promotes migration and invasion by activating PI3K/AKT and MEK/ERK1/2 signaling pathways via CXCL8-CXCR1/2 signaling. A, B Representative images and statistical analysis of

migration and invasion in KYSE-450 shNC/shACC1 and KYSE-150 shNC/shACC1 cells following LY294002 treatment. **C, D** Representative images and statistical analysis of migration and invasion in KYSE-450 shNC/shACC1 and KYSE-150 shNC/shACC1 cells following U0126 treatment. **E, F** Immunoblot analysis showing the effects of LY294002 and U0126 on the levels of p-AKT, p-ERK1/2, and EMT marker proteins in KYSE-450 and KYSE-150 shNC/shACC1 cells. Each experiment was repeated thrice. Data are presented as mean ± SD. Significance levels are indicated as follows: $*P < 0.05$, $**P < 0.01$, $***P < 0.001$.

Supplementary Figure 4

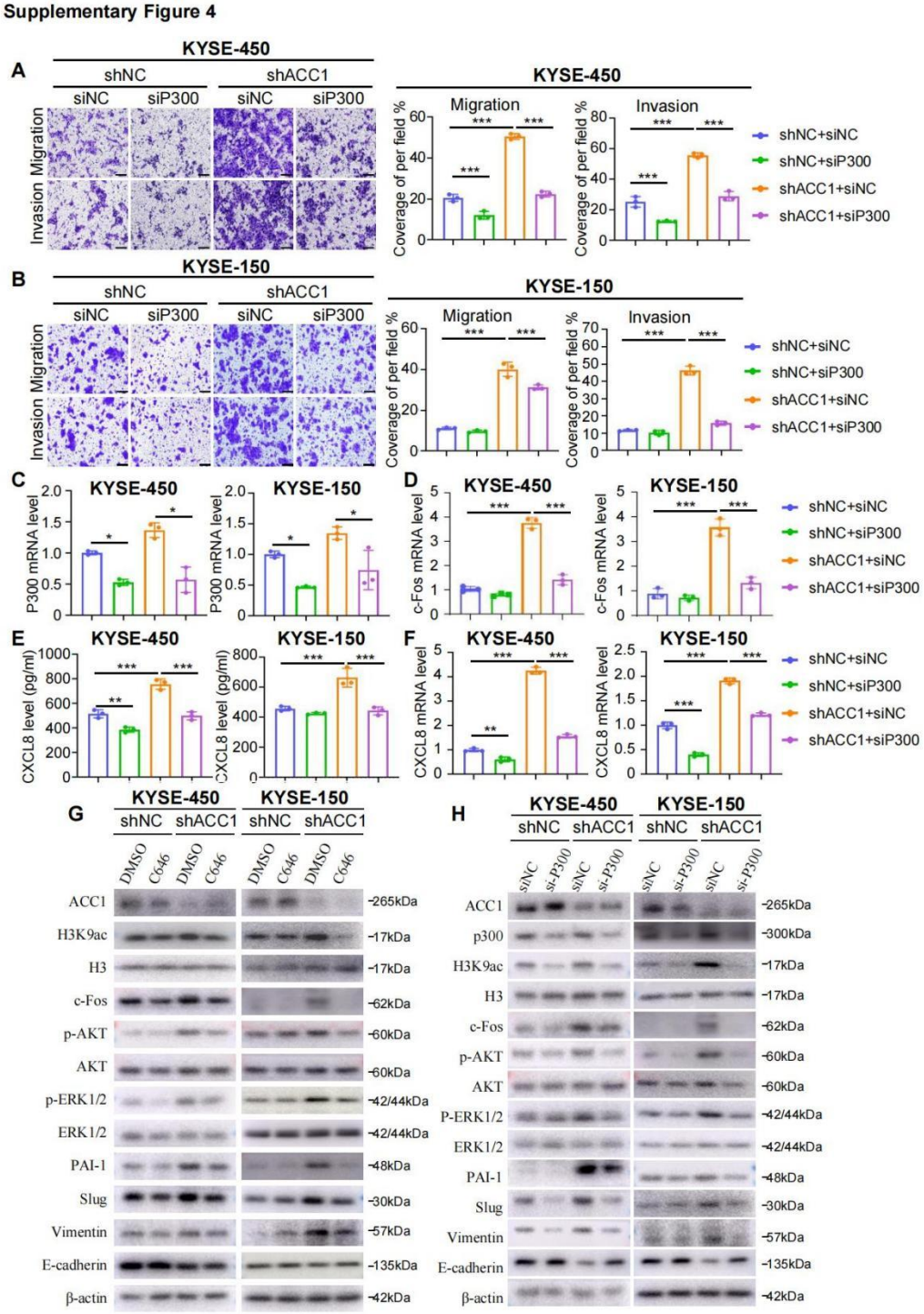

Supplementary Figure 4: ACC1 knockdown increases c-Fos and CXCL8 levels via a histone acetylation mechanism. A, B Representative images and statistical analysis of migration and invasion in KYSE-450 and KYSE-150 shNC/shACC1 cells

after p300 knockdown. **C** RT-qPCR analysis of *p300* knockdown efficiency. **D** RT-qPCR analysis of *c-Fos* levels in KYSE-450 and KYSE-150 shNC/shACC1 cells after p300 knockdown. **E** qPCR and ELISA assays of CXCL8 levels in KYSE-450 and KYSE-150 shNC/shACC1 cells after p300 knockdown. **F** RT-qPCR analysis of *CXCL8* levels in KYSE-450 and KYSE-150 shNC/shACC1 cells after p300 knockdown. **G** Immunoblot analysis showing the effects of C646 on H3K9ac, c-Fos, p-AKT, p-ERK1/2, and EMT marker protein levels in KYSE-450 and KYSE-150 shNC/shACC1 cells. **H** Immunoblot analysis showing the effects of siP300 on H3K9ac, c-Fos, p-AKT, p-ERK1/2, and EMT marker protein levels in KYSE-450 and KYSE-150 shNC/shACC1 cells. Each experiment was repeated thrice. Data are presented as mean ± SD. Significance levels are indicated as follows: $*P < 0.05$, $**P < 0.01$, $***P < 0.001$.

Supplementary Figure 5

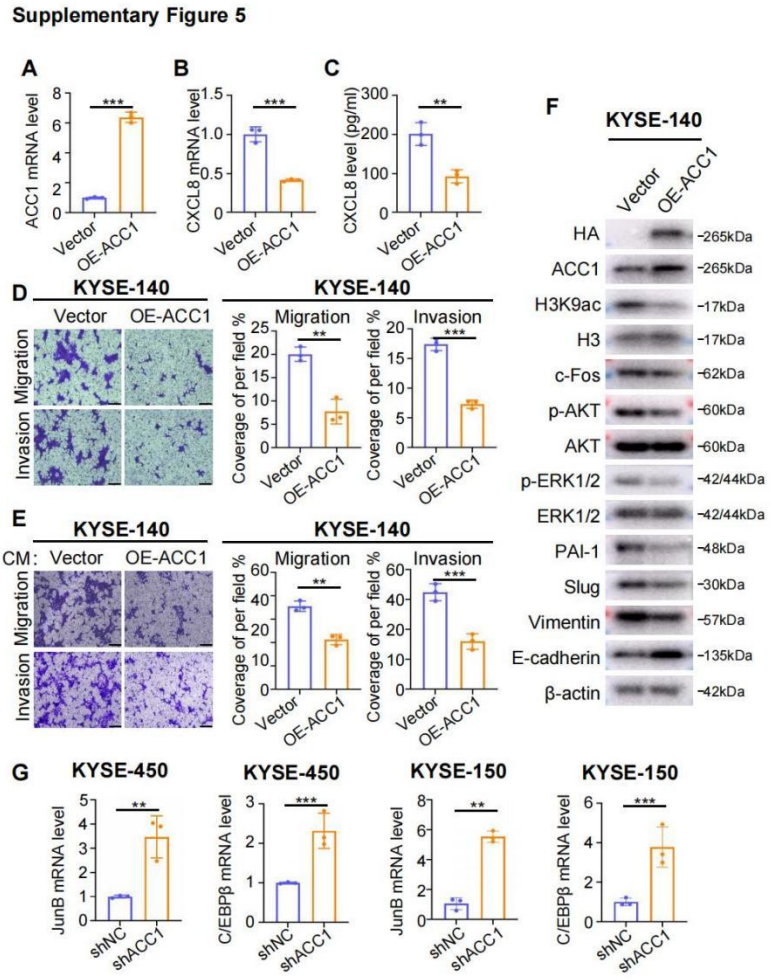

Supplementary Figure 5: ACC1 overexpression inhibits ESCC cell migration and invasion. A RT-qPCR analysis of *ACC1* overexpression efficiency in KYSE-140 cells. **B** RT-qPCR analysis of *CXCL8* expression levels in KYSE-140 cells with vector control (vector) or ACC1 overexpression (OE-ACC1). **C** ELISA analysis of CXCL8 levels in the CM from KYSE-140 vector and OE-ACC1 cells. **D** Representative images and statistical analysis of migration and invasion in KYSE-140 vector and OE-ACC1 cells. **E** Representative images and statistical analysis of the

494 effect of CM from KYSE-140 vector and OE-ACC1 cells on migration and invasion
495 in KYSE-140 cells. **F** Immunoblot analysis showing the effects of ACC1
496 overexpression on the levels of H3K9ac, c-Fos, p-ERK1/2, p-AKT, H3ac, and EMT
497 marker proteins in KYSE-140 cells. **G** RT-qPCR analysis of *JunB* and *C/EBPβ*
498 mRNA levels in KYSE-450 and KYSE-150 shNC/shACC1 cells. Each experiment
499 was repeated thrice. Data are presented as mean± SD. Significance levels are
500 indicated as follows: *$P < 0.05$, **$P < 0.01$, ***$P < 0.001$.

501

502

503

504

505

506

507

508

509

510

Supplementary Figure 6

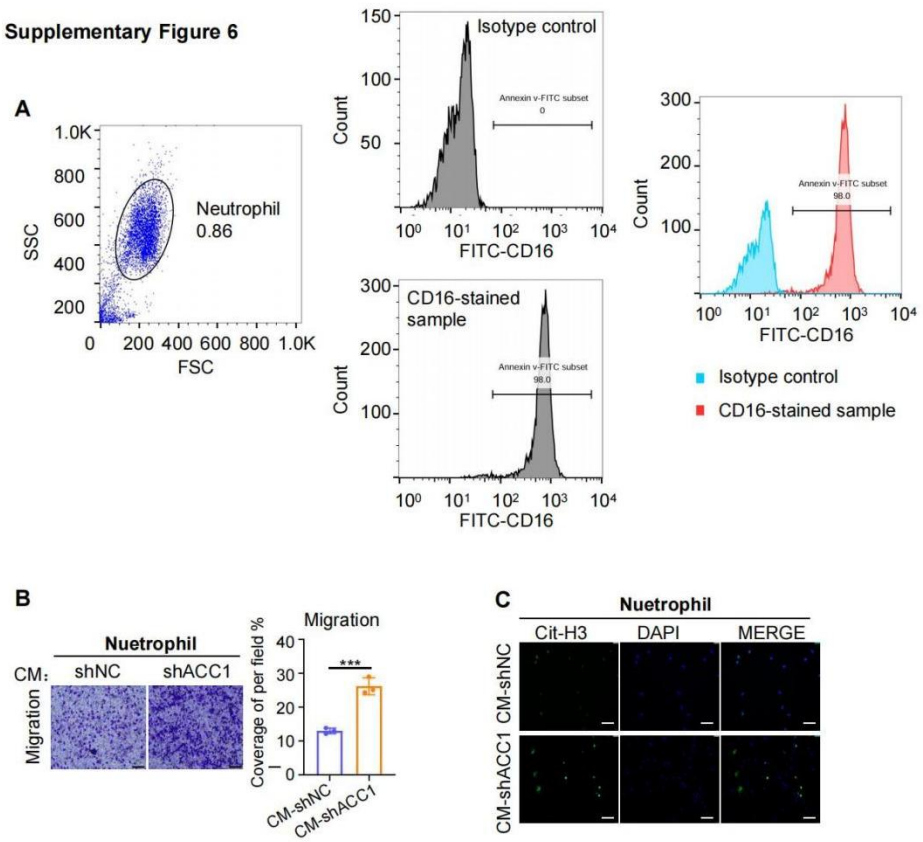

Supplementary Figure 6: ACC1 knockdown in ESCC cells facilitates neutrophil recruitment and NETs formation via CXCL8 produced from tumor cells. A Flow cytometry analysis confirming the purity of neutrophil populations. **B** Representative images and statistical analysis of neutrophil migration induced by conditional medium (CM) from KYSE-450 shNC and shACC1 cells. **C** Representative fluorescence microscopy images showing the effect of CM from KYSE-450 shNC and shACC1 cells on neutrophil extracellular traps (NET), with NETs co-stained for citrullinated histone H3 (cit-H3) and DAPI. Scale bar, 25 μm. Data represent mean ± SD. *$P < 0.05$, **$P < 0.01$, ***$P < 0.001$.

Supplementary Figure 7

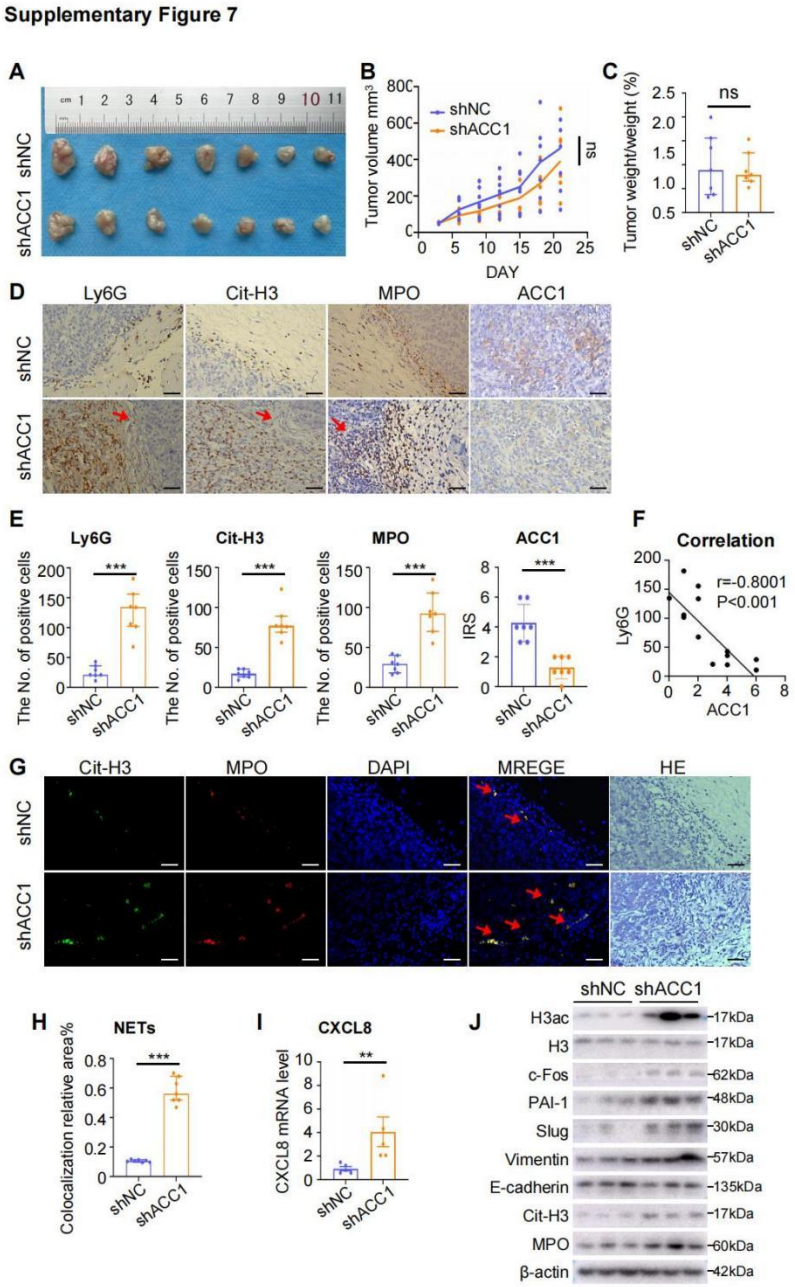

Supplementary Figure 7: ACC1 knockdown promotes neutrophil infiltration, NETs formation, and invasive behavior in ESCC xenograft tumors. A Images of tumors derived from KYSE-150 shNC and shACC1 cells. **B** Tumor growth curves over the course of the experiment. **C** Statistical analysis of tumor weight as a percentage of total body weight at the end of the experiment. **D** Representative images

of immunohistochemistry (IHC) staining for Ly6G, cit-H3, MPO, and ACC1 in tumor tissues. **E** Quantification of Ly6G, cit-H3, and MPO positive cells, and ACC1 IHC immunoreactivity score (IRS). **F** Correlation analysis between the numbers of Ly6G positive cells and ACC1 levels. **G** Representative images of immunofluorescence (IF) staining for NETs, with NETs co-stained for cit-H3 (green) and MPO (red). **H** Quantification of the overlapping area of cit-H3 and MPO staining. **I** RT-qPCR analysis of *CXCL8* mRNA levels in tumor tissues from shNC and shACC1 groups. **J** Western blot analysis of H3K9ac, c-Fos, p-AKT, p-ERK1/2, cit-H3, MPO, and EMT marker protein levels in tumor tissues from shNC and shACC1 groups. Spearman method was used for correlation analysis. n = 7. Scale bar, 25 μm. No., number. Data represent mean ± SEM. **P* < 0.05, ***P* < 0.01, ****P* < 0.001.

Supplementary Figure 8

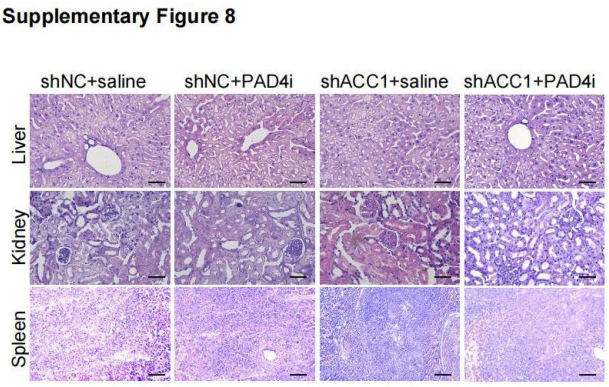

Supplementary Figure 8: ACC1 knockdown drives ESCC metastasis via NETs in vivo. Hematoxylin and eosin (HE) staining of liver, kidney and spleen tissue form each group of tail vein mouse models treated with saline or PAD4i. Scale bar, 25 μm.

Supplementary Figure 9

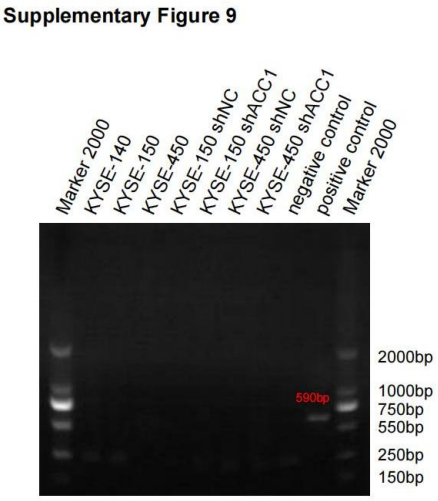

Supplementary Figure 9: Agarose gel electrophoresis result confirmed that none of the analyzed ESCC cell lines exhibited mycoplasma contamination. Nested Polymerase Chain Reaction (Nested PCR) was performed to examine mycoplasma in the KYSE-140, KYSE-150, KYSE-450, KYSE-150 shNC/shACC1, and KYSE-450 shNC/shACC1 cell lines, with a positive control of 590 bp included.

Supplementary Table 1

Clinicopathological correlation of ACC1 mRNA expression in ESCC tumor tissues

Clinical characteristics	Case	ACC1 expression		χ^2	*P* value
		Low group	High group		
Age (years old)				1.4792	0.2239
≤ 65	53	23 (46.94%)	30 (61.22%)		
> 65	45	26 (53.06%)	19 (38.78%)		
Gender				0.0552	0.8143
Female	24	11 (22.45%)	13 (26.53%)		
Male	74	38 (77.55%)	36 (73.47%)		
Clinical stage				52.587	**< 0.0001**
I	25	24 (48.98%)	1 (2.04%)		
II	42	4 (8.16%)	38 (77.55%)		
III	31	21 (42.86%)	10 (20.41%)		
Tumor invasion				16.1469	**0.0003**
T_1	12	12 (24.49%)	0 (0%)		
T_2	27	15 (30.61%)	12 (24.49%)		
T_3	59	22 (44.9%)	37 (75.51%)		
Lymph node metastasis				6.4625	**0.0395**
N_0	67	28 (57.14%)	39 (79.59%)		
N_1	22	16 (32.65%)	6 (12.24%)		
N_2	9	5 (10.2%)	4 (8.16%)		
Size				3.3075	0.069
> 5	50	20 (40.82%)	30 (61.22%)		
≤ 5	48	29 (59.18%)	19 (38.78%)		
Location				1.9082	0.3852
Lower	22	9 (18.37%)	13 (26.53%)		
Middle	70	38 (77.55%)	32 (65.31%)		
Upper	6	2 (4.08%)	4 (8.16%)		
Grade				4.0341	0.4014
High	41	25 (51.02%)	16 (32.65%)		
Low	9	4 (8.16%)	5 (10.2%)		
Middle	38	16 (32.65%)	22 (44.9%)		
Middle-high	4	1 (2.04%)	3 (6.12%)		
Middle-low	6	3 (6.12%)	3 (6.12%)		

Supplementary Table 2

Clinicopathological correlation of ACC1 levels in ESCC tumor tissues

Clinical characteristics	Case	ACC1 level		χ^2	*P* value
		Low group	High group		
Age (years old)				1.8546	0.1732
≤ 65	52	30 (65.22%)	22 (48.89%)		
> 65	39	16 (34.78%)	23 (51.11%)		
Gender				0.5278	0.4675
Female	38	17 (36.96%)	21 (46.67%)		
Male	53	29 (63.04%)	24 (53.33%)		
Clinical stage				1.397	0.7062
I	7	4 (8.7%)	3 (6.67%)		
II	67	33 (71.74%)	34 (75.56%)		
III	16	9 (19.57%)	7 (15.56%)		
IV	1	0 (0%)	1 (2.22%)		
Tumor invasion				1.4712	0.4792
T_1	6	4 (8.7%)	2 (4.44%)		
T_2	20	11 (23.91%)	9 (20%)		
T_3	65	31 (67.39%)	34 (75.56%)		
Lymph node metastasis				2.0448	0.5632
N_0	72	35 (76.09%)	37 (82.22%)		
N_1	12	7 (15.22%)	5 (11.11%)		
N_2	6	4 (8.7%)	2 (4.44%)		
N_3	1	0 (0%)	1 (2.22%)		
Size				0.8801	0.3482
> 5	39	17 (36.96%)	22(48.89%)		
≤ 5	51	29 (63.04%)	22(50%)		
Location				2.4702	0.2908
Lower	18	12 (26.09%)	6 (13.33%)		
Middle	61	29 (63.04%)	32 (71.11%)		
Upper	12	5 (10.87%)	7 (15.56%)		
Grade				10.9689	0.052
High	34	23 (50%)	11 (24.44%)		
Low	8	2 (4.35%)	6 (13.33%)		
Middle	37	17 (36.96%)	20 (44.44%)		
Middle-high	8	3 (6.52%)	5 (11.9%)		
Middle-low	1	1 (2.38%)	0 (0%)		

Supplementary Table 3

Clinicopathological correlation of CXCL8 mRNA expression in ESCC tumor tissues

Clinical characteristics	Case	CXCL8 expression		χ^2	*P* value
		Low group	High group		
Age (years old)				0.6574	0.4175
≤ 65	53	29 (59.18%)	24 (48.98%)		
> 65	45	20 (40.82%)	25 (51.02%)		
Gender				0	1
Female	24	12 (24.49%)	12 (24.49%)		
Male	74	37 (75.51%)	37 (75.51%)		
Clinical stage				24.3775	**< 0.0001**
I	25	6 (12.24%)	19 (38.78%)		
II	42	33 (67.35%)	9 (18.37%)		
III	31	10 (20.41%)	21 (42.86%)		
Tumor invasion				2.4972	0.2869
T_1	12	4 (8.16%)	8 (16.33%)		
T_2	27	12 (24.49%)	15 (30.61%)		
T_3	59	33 (67.35%)	26 (53.06%)		
Lymph node metastasis				6.4625	**0.0395**
N_0	67	39 (79.59%)	28 (57.14%)		
N_1	22	6 (12.24%)	16 (32.65%)		
N_2	9	4 (8.16%)	5 (10.2%)		
Size				2.0008	0.1572
> 5	50	29 (59.18%)	21 (42.86%)		
≤ 5	48	20 (40.82%)	28 (57.14%)		
Location				1.9082	0.3852
Lower	22	13 (26.53%)	9 (18.37%)		
Middle	70	32 (65.31%)	38 (77.55%)		
Upper	6	4 (8.16%)	2 (4.08%)		
Grade				9.1043	0.0585
High	41	16 (32.65%)	25 (51.02%)		
Low	9	7 (14.29%)	2 (4.08%)		
Middle	38	23 (46.94%)	15 (30.61%)		
Middle-high	4	2 (4.08%)	2 (4.08%)		
Middle-low	6	1 (2.04%)	5 (10.2%)		

Supplementary Table 4

Clinicopathological correlation of NETs levels in ESCC tumor tissues

Clinical characteristics	Case	NETs level		χ^2	*P* value
		Low group	High group		
Age (years old)				0.2647	0.6069
≤ 65	52	28 (60.87%)	24 (53.33%)		
> 65	39	18 (39.13%)	21 (46.67%)		
Gender					
Female	38	21 (45.65%)	17 (37.78%)	0.3014	0.583
Male	53	25 (54.35%)	28 (62.22%)		
Clinical stage				2.1471	0.5425
I	7	3 (6.52%)	4 (8.89%)		
II	67	33 (71.74%)	34 (75.56%)		
III	16	10 (21.74%)	6 (13.33%)		
IV	1	0 (0%)	1 (2.22%)		
Tumor invasion				0.2044	0.9028
T_1	6	3 (6.52%)	3 (6.67%)		
T_2	20	11 (23.91%)	9 (20%)		
T_3	65	32 (69.57%)	33 (73.33%)		
Lymph node metastasis				3.2116	0.3601
N_0	72	34 (73.91%)	38 (84.44%)		
N_1	12	8 (17.39%)	4 (8.89%)		
N_2	6	4 (8.7%)	2 (4.44%)		
N_3	1	0 (0%)	1 (2.22%)		
Size				0.372	0.5419
> 5	39	18 (39.13%)	21 (47.73%)		
≤ 5	51	28 (60.87%)	23 (52.27%)		
Location				0.3388	0.8442
Lower	18	9 (19.57%)	9 (20%)		
Middle	61	30 (65.22%)	31 (68.89%)		
Upper	12	7 (15.22%)	5 (11.11%)		
Grade				3.3171	0.5062
High	34	18 (40%)	16 (37.21%)		
Low	8	4 (8.89%)	4 (9.3%)		
Middle	37	20 (44.44%)	17 (39.53%)		
Middle-high	8	2 (4.44%)	6 (13.95%)		
Middle-low	1	1 (2.22%)	0 (0%)		

Supplementary Table 5

Clinicopathological correlation of NETs levels in ESCC tumor adjacent tissues

Clinical characteristics	Case	NETs level		χ^2	*P* value
		Low group	High group		
Age (years old)				0.0082	0.9277
≤ 65	52	27 (58.7%)	25 (55.56%)		
> 65	39	19 (41.3%)	20 (44.44%)		
Gender				0.3014	0.583
Female	38	21 (45.65%)	17 (37.78%)		
Male	53	25 (54.35%)	28 (62.22%)		
Clinical stage				4.0066	0.2608
I	7	2 (4.35%)	5 (11.11%)		
II	67	37 (80.43%)	30 (66.67%)		
III	16	6 (13.04%)	10 (22.22%)		
IV	1	1 (2.17%)	0 (0%)		
Tumor invasion				1.4712	0.4792
T_1	6	2 (4.35%)	4 (8.89%)		
T_2	20	12 (26.09%)	8 (17.78%)		
T_3	65	32 (69.57%)	33 (73.33%)		
Lymph node metastasis				2.2115	0.5297
N_0	72	38 (82.61%)	34 (75.56%)		
N_1	12	5 (10.87%)	7 (15.56%)		
N_2	6	2 (4.35%)	4 (8.89%)		
N_3	1	1 (2.17%)	0 (0%)		
Size				1.0722	0.3004
> 5	39	17(36.96%)	22(50%)		
≤ 5	51	29(63.04%)	22(50%)		
Location				1.6923	0.4291
Lower	18	10 (21.74%)	8 (17.78%)		
Middle	61	32 (69.57%)	29 (64.44%)		
Upper	12	4 (8.7%)	8 (17.78%)		
Grade				3.1267	0.5368
High	34	20 (43.48%)	14 (33.33%)		
Low	8	3 (6.52%)	5 (11.9%)		
Middle	37	20 (43.48%)	17 (40.48%)		
Middle-high	8	3 (6.52%)	5 (11.9%)		
Middle-low	1	0 (0%)	1 (2.38%)		

Supplementary Table 6

STR profiling for cell line authentication

Cells for Testing	Multiple Alleles	Matched Cell Line	Cell Bank	EV	Description
KYSE-140	None	KYSE-140	DSMZ	1.0	Full Match
KYSE-450-shNC	None	KYSE-450	DSMZ	1.0	Full Match
KYSE-450-shACC1	None	KYSE-450	DSMZ	1.0	Full Match
KYSE-150-shNC	None	KYSE-150	DSMZ	1.0	Full Match
KYSE-150-shACC1	None	KYSE-150	DSMZ	1.0	Full Match

Fig. 2: A

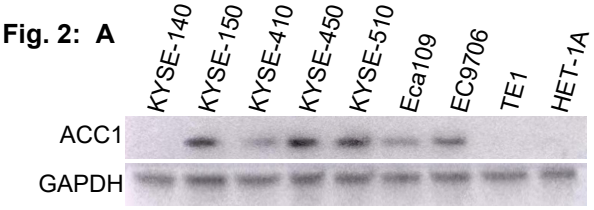

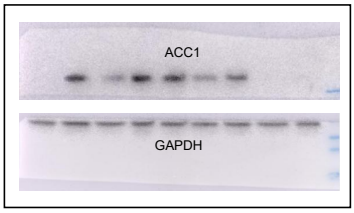

Fig. S2: A

KYSE-450

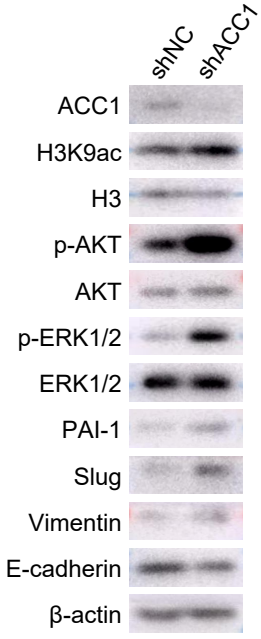

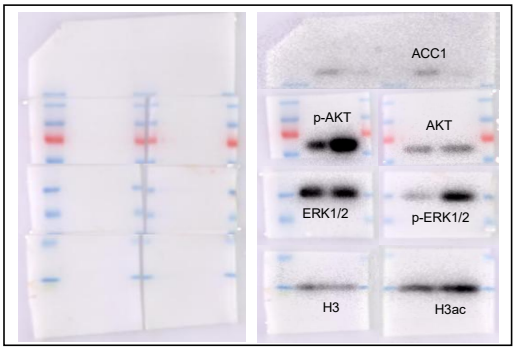

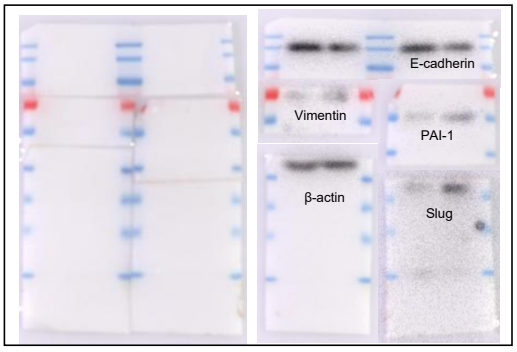

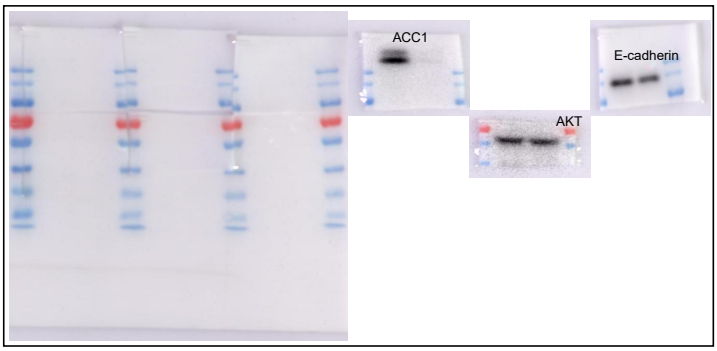

Fig. S2: A

KYSE-150

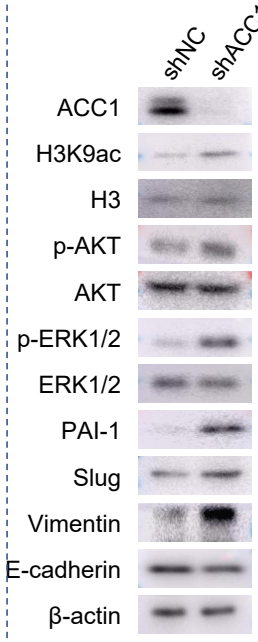

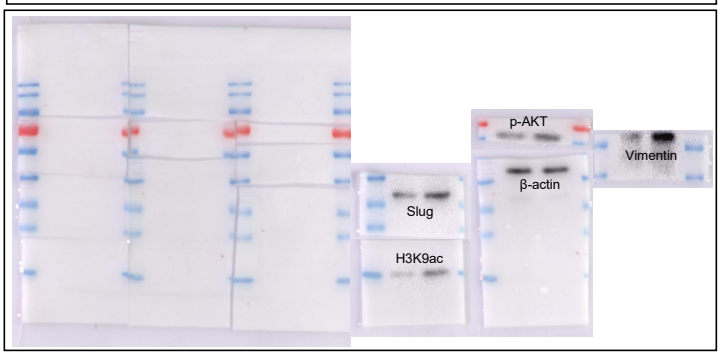

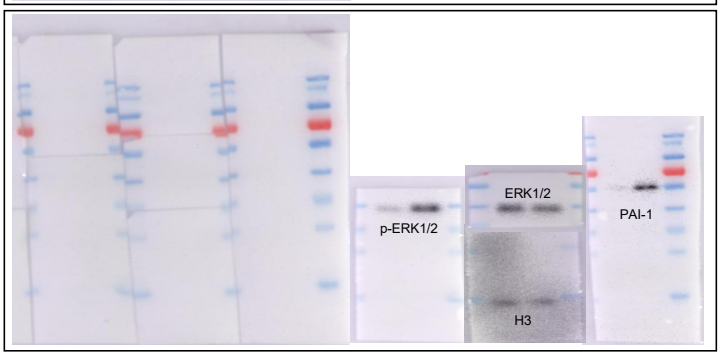

Fig. S2: B

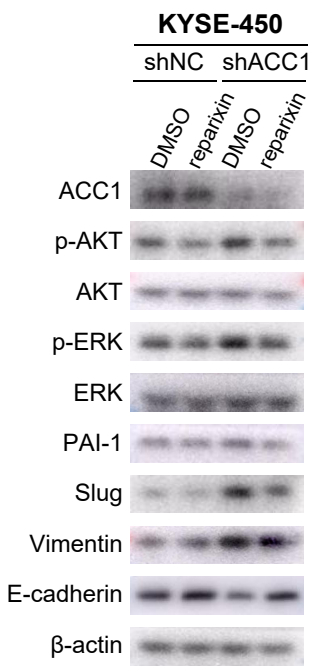

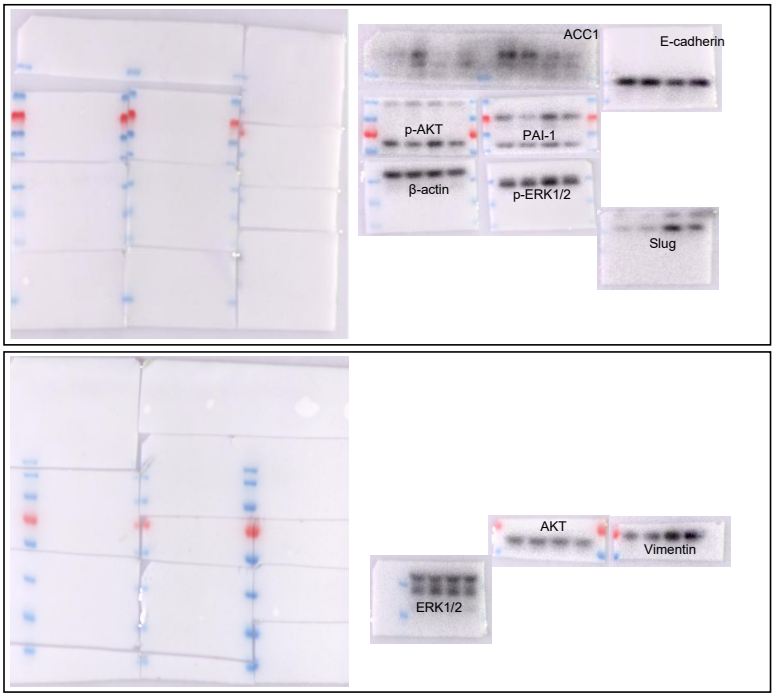

Fig. S2: B

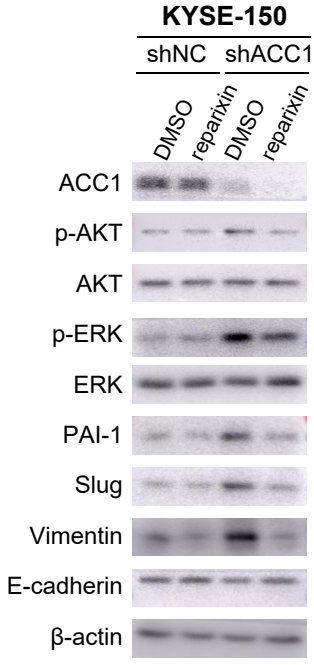

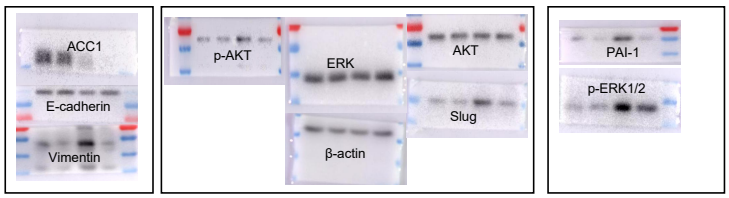

Fig. S2: B

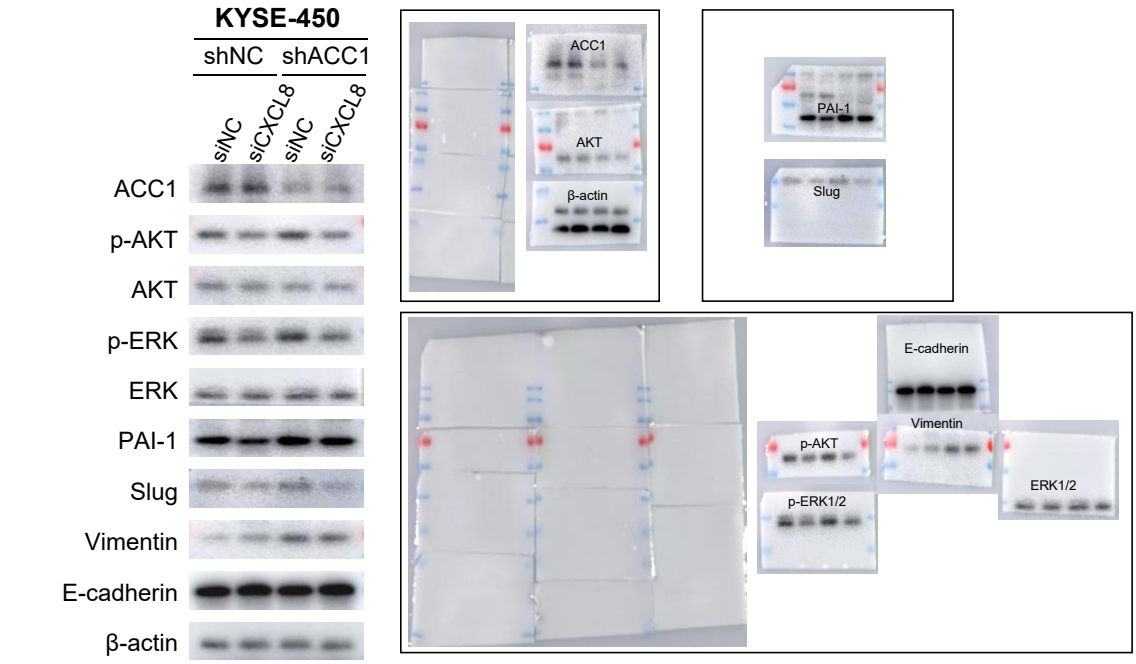

Fig. S2: B

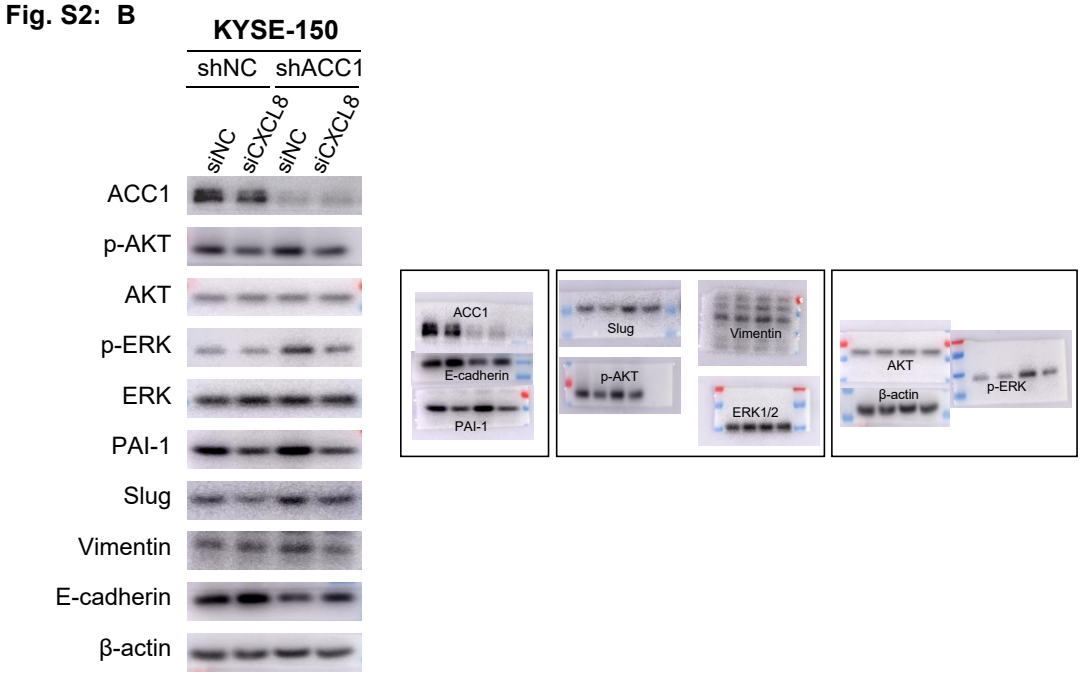

Fig. S2: C

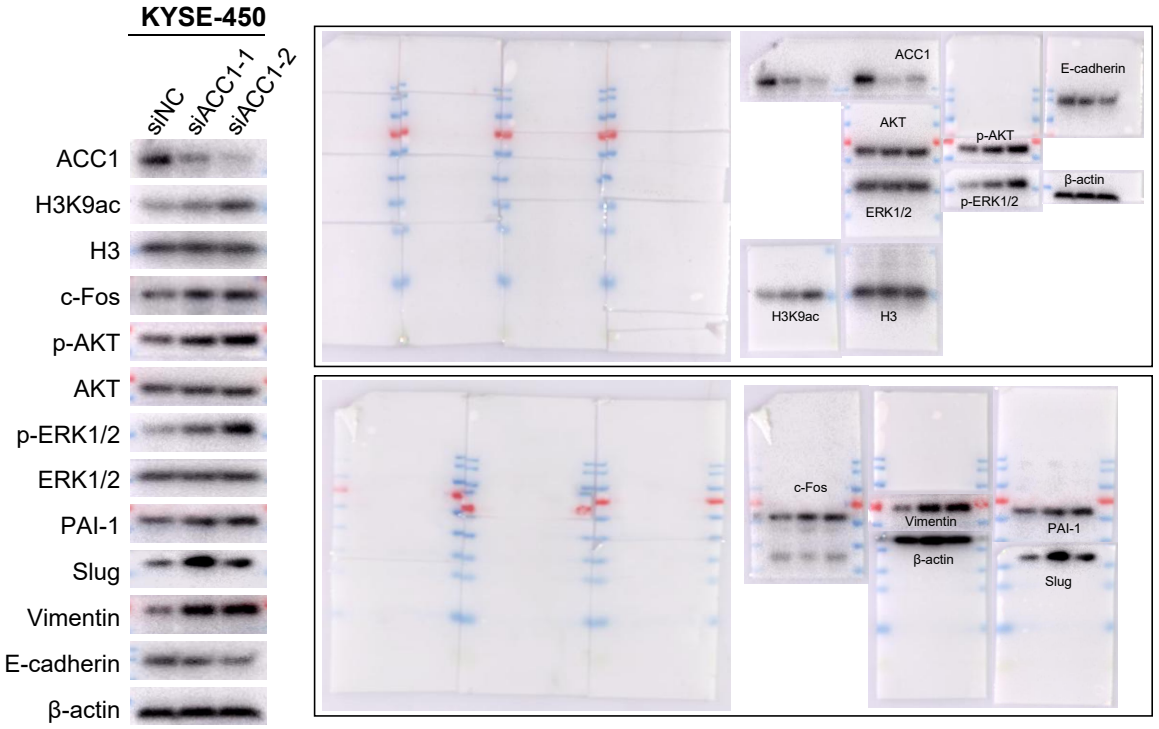

Fig. S2: C

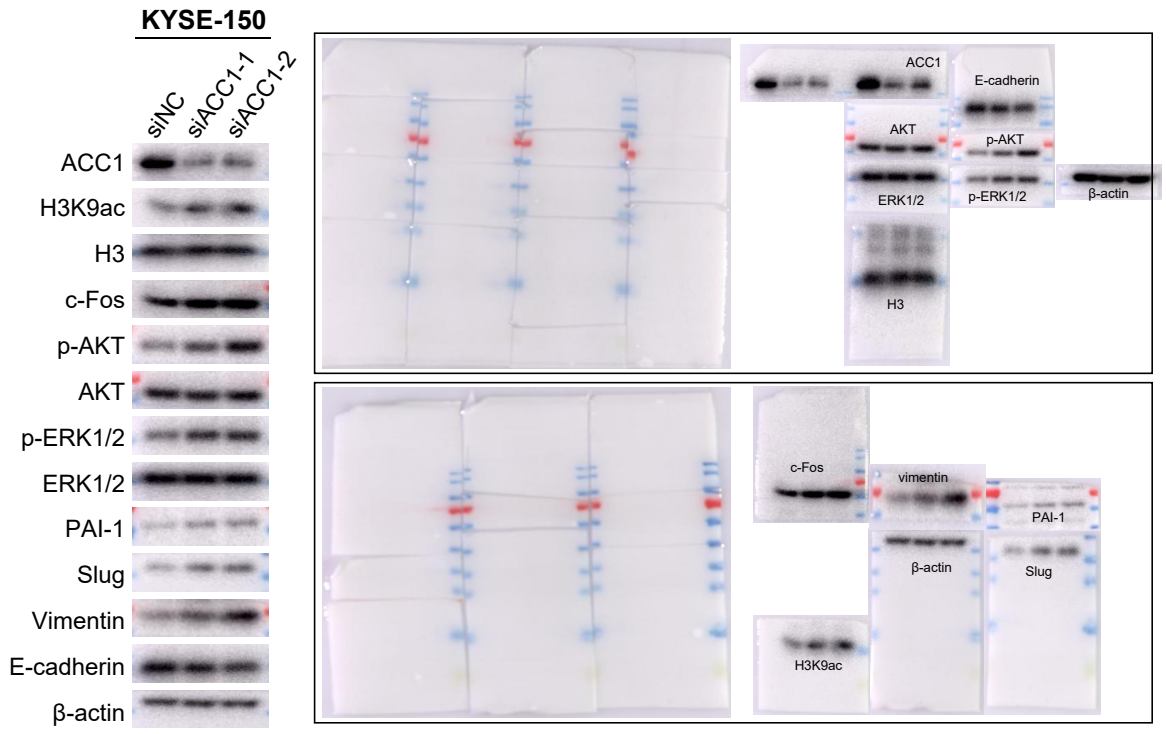

Fig. S3: E

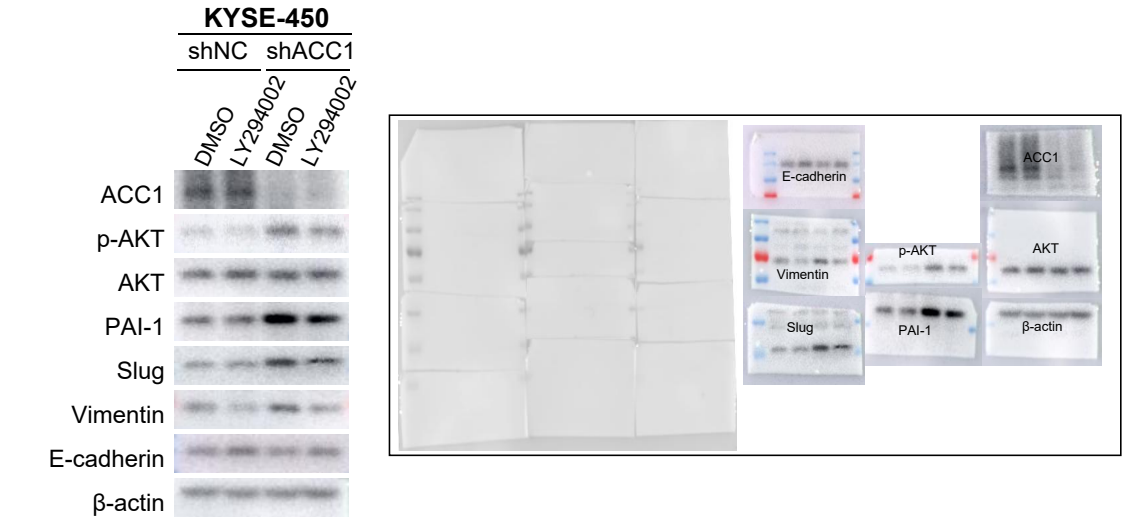

Fig. S3: E

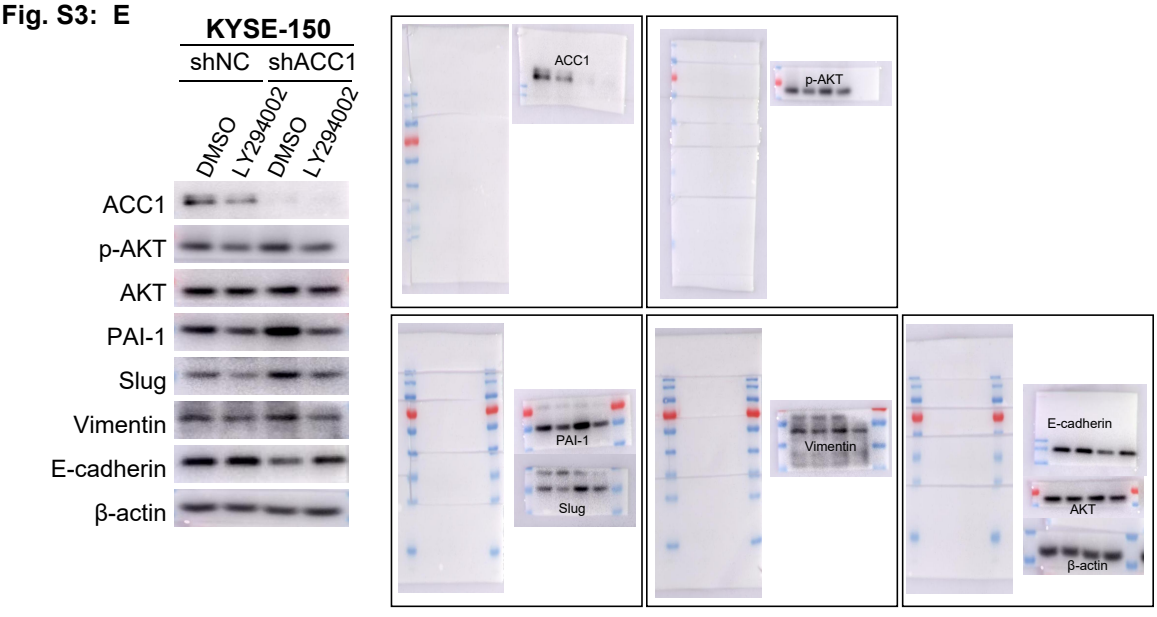

Fig. S3: F

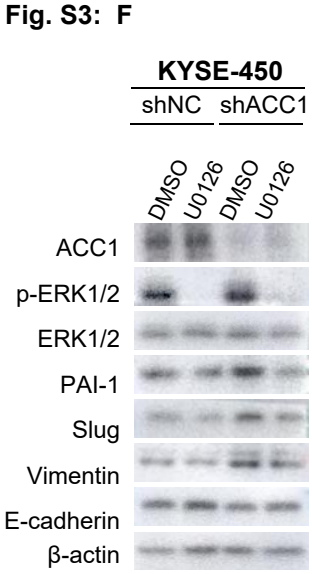

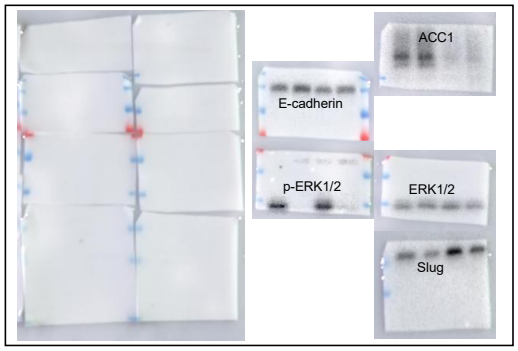

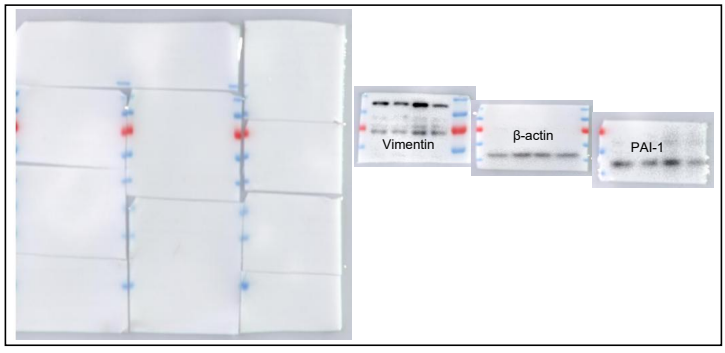

Fig. S3: F

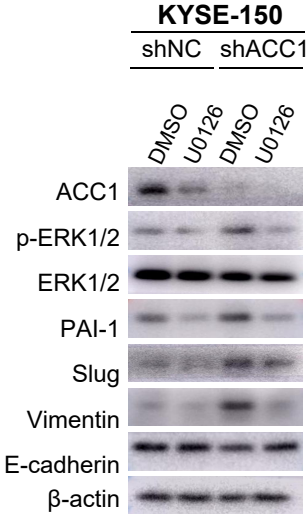

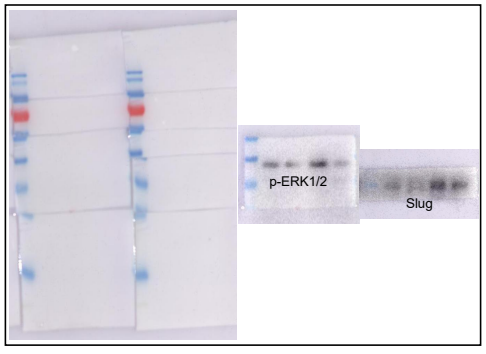

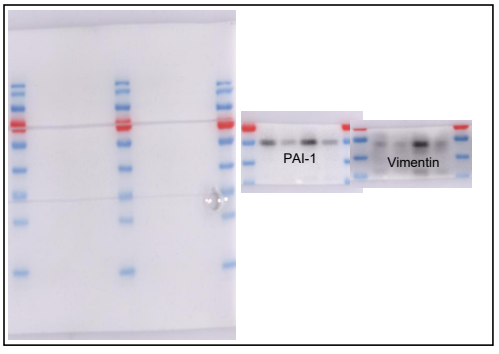

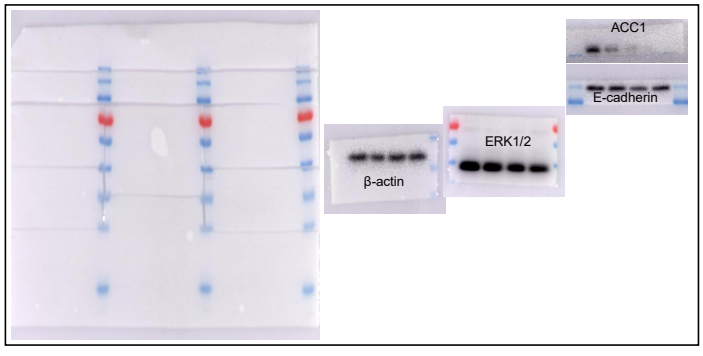

Fig. 4: I

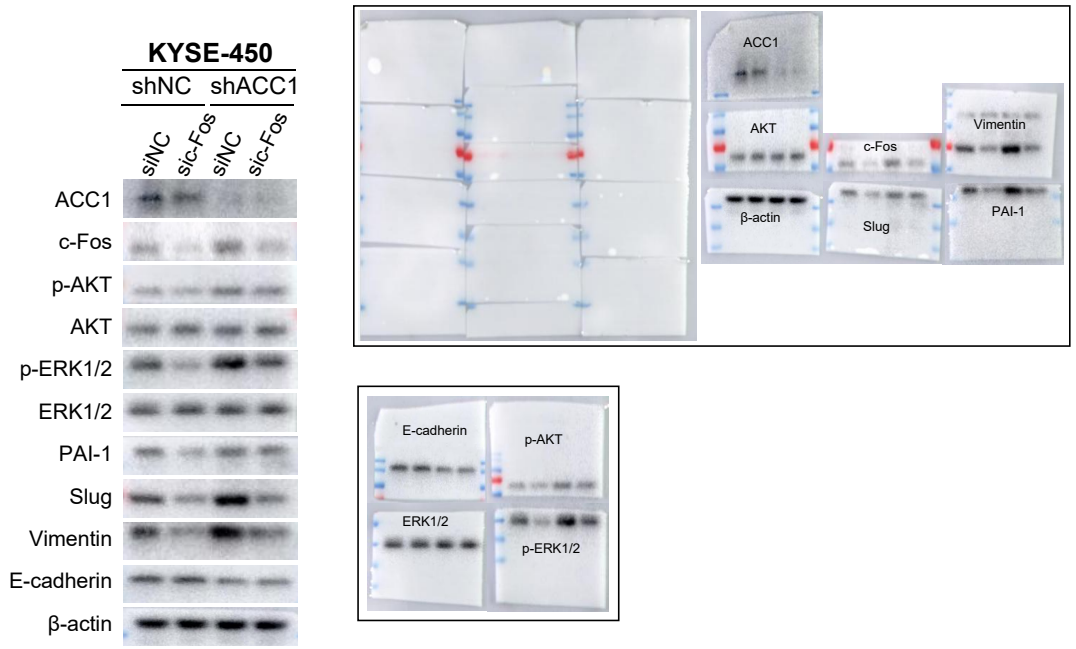
KYSE-450
shNC
shACC1
siNC
sic-Fos
siNC
sic-Fos
ACC1
c-Fos
p-AKT
AKT
p-ERK1/2
ERK1/2
PAI-1
Slug
Vimentin
E-cadherin
β-actin
ACC1
AKT
c-Fos
Vimentin
β-actin
Slug
PAI-1
E-cadherin
p-AKT
ERK1/2
p-ERK1/2

Fig. 4: I

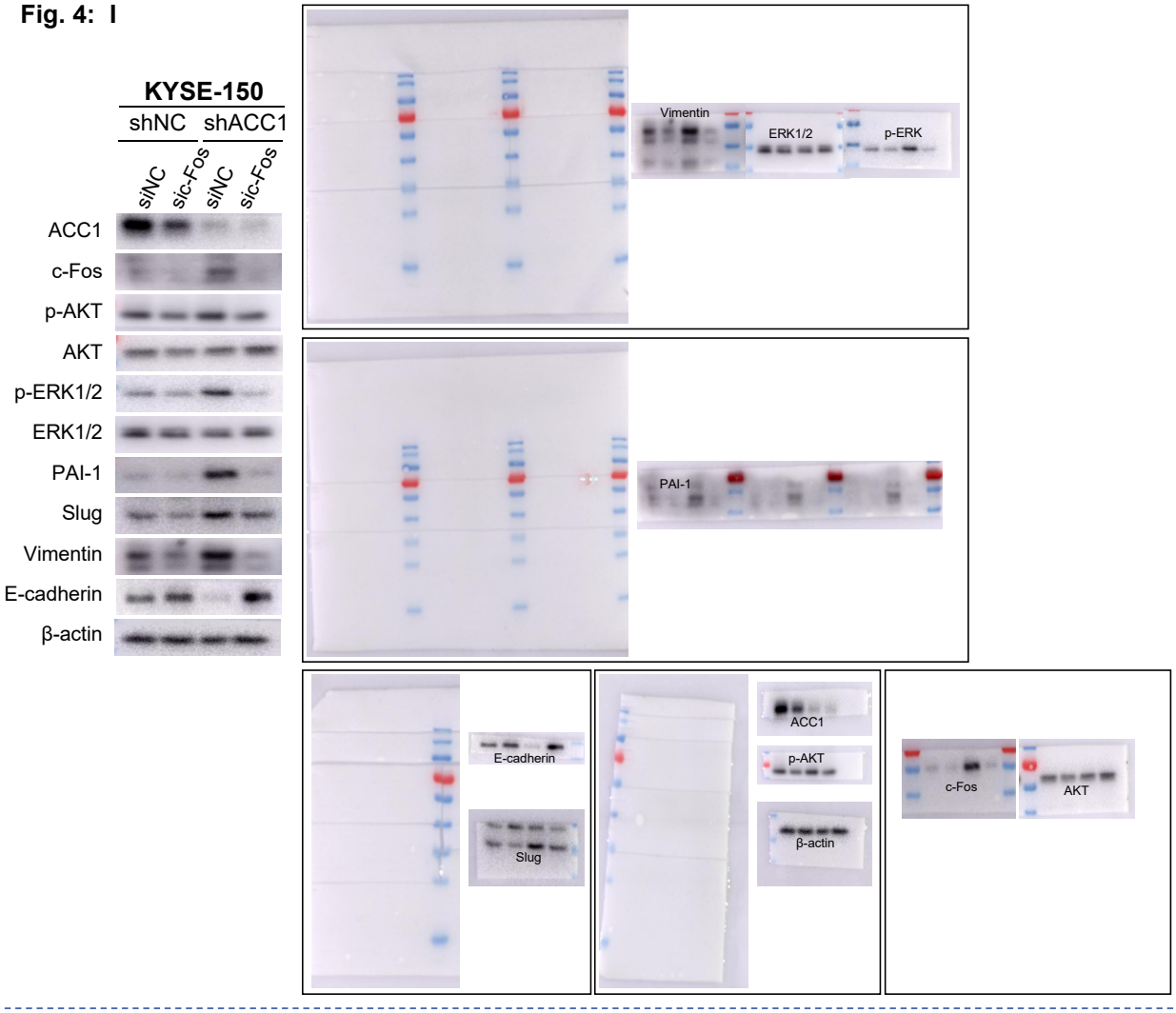
KYSE-150
shNC
shACC1
siNC
sic-Fos
siNC
sic-Fos
ACC1
c-Fos
p-AKT
AKT
p-ERK1/2
ERK1/2
PAI-1
Slug
Vimentin
E-cadherin
β-actin
Vimentin
ERK1/2
p-ERK
PAI-1
E-cadherin
Slug
ACC1
p-AKT
β-actin
c-Fos
AKT

Fig. S4: G

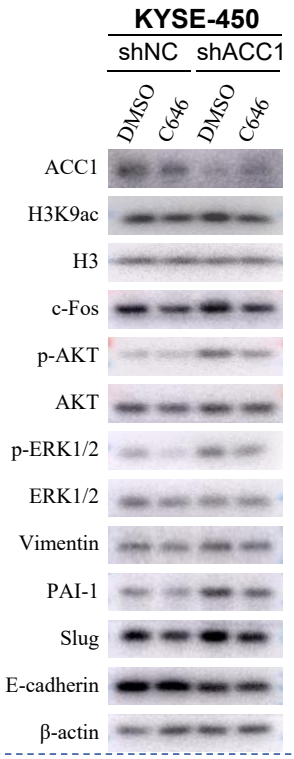

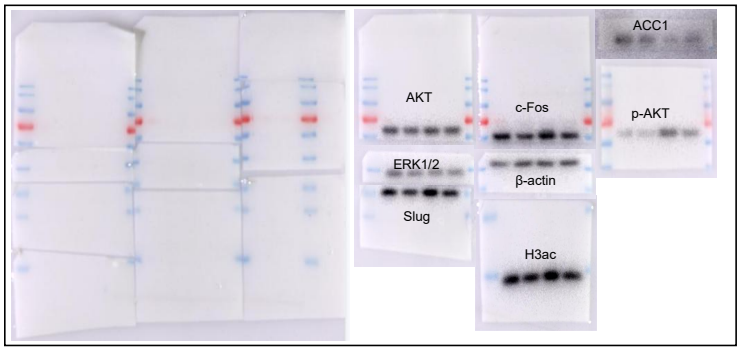

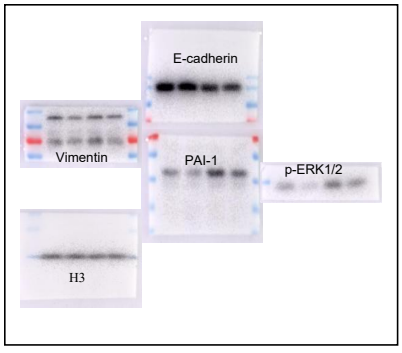

Fig. S4: G

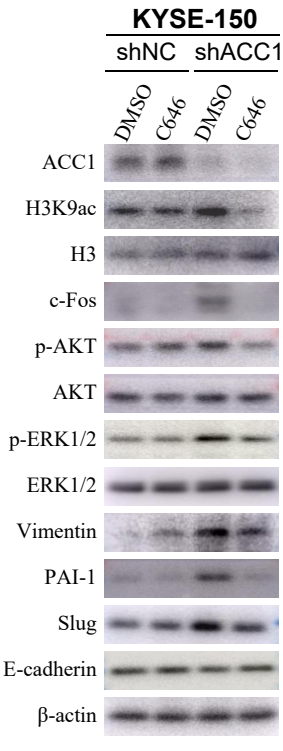

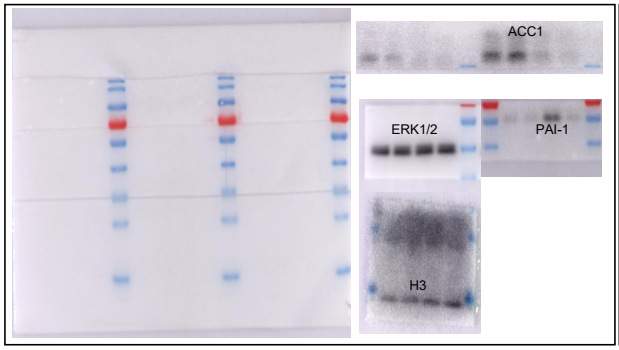

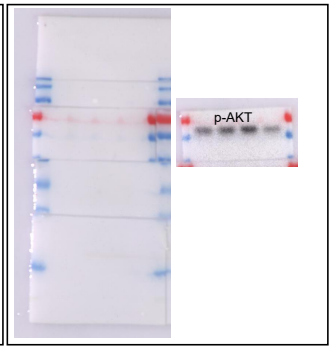

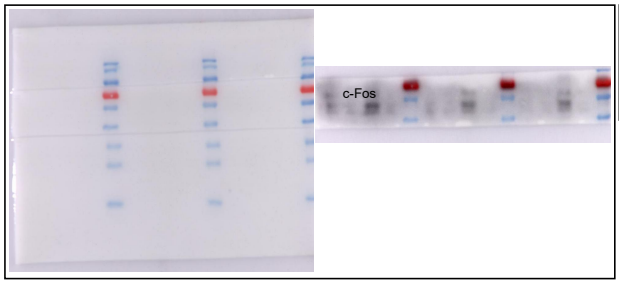

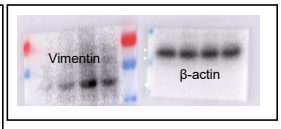

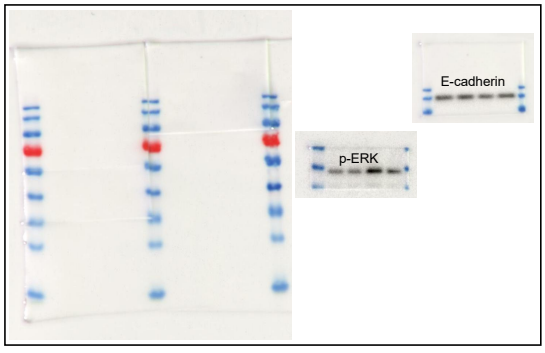

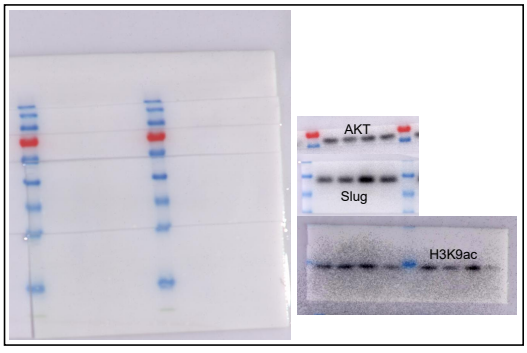

Fig. S4: H

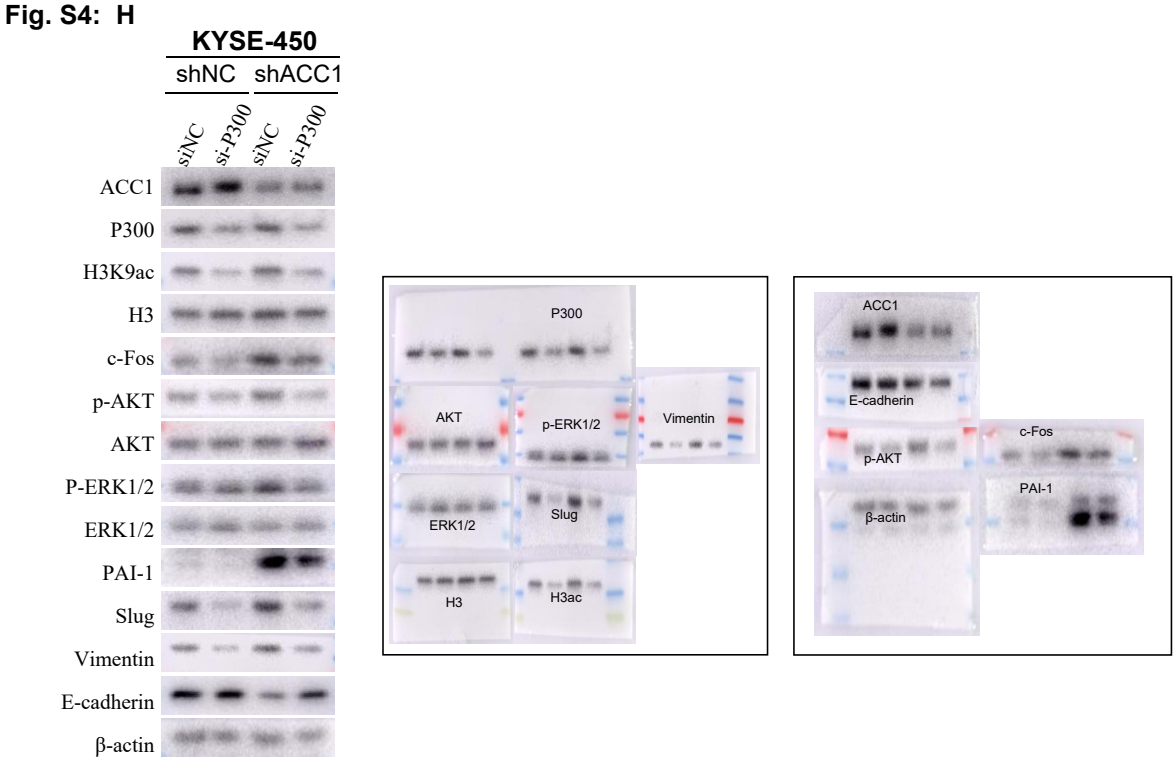

Fig. S4: H

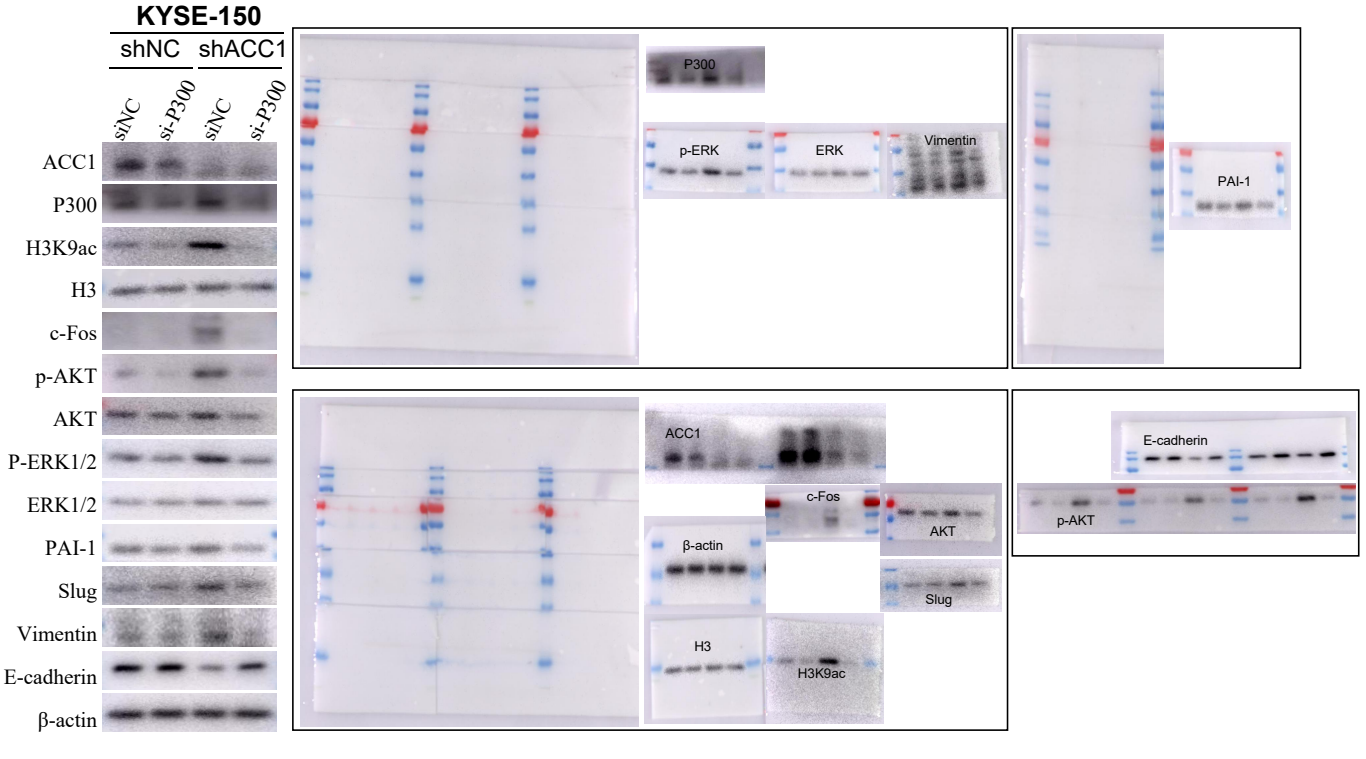

Fig. S5: F

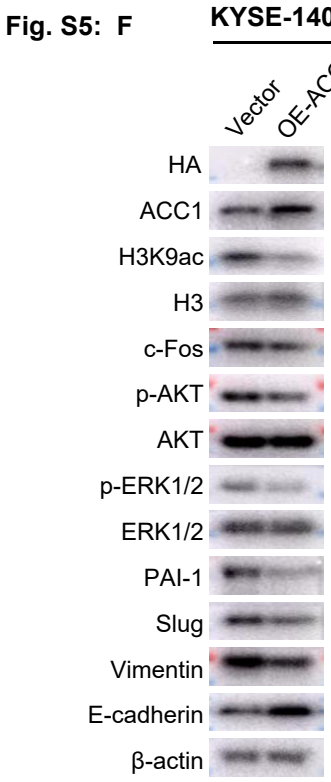

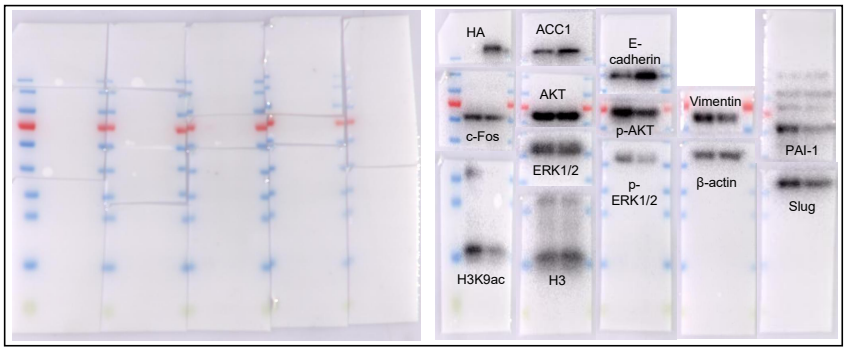

Fig. S7: J